RSC Applied Polymers

PAPER

View Article Online
View Journal | View Issue

Check for updates

Cite this: *RSC Appl. Polym.*, 2025, **3**, 1508

Structure–function correlation of branched and linear polyaramides for the removal of pollutants from water

Gomathi Mahadevan and Suresh Valiyaveettil *

Plastic waste materials in the environment degrade and release smaller particles called microplastic and nanoplastic particles. In this study, a series of polyaramides (PAs) are prepared with different structural features and used to remove plastic nanoparticles and dissolved dyes. The prepared PAs showed good thermal stability, high surface area, and negative zeta surface potential, which were useful for the extraction of pollutants. Among the six PAs studied, PA3 showed the highest adsorption capacity of 342.54 mg g^{-1} towards cationic polyvinyl chloride nanoparticles (PVC NPs) and dissolved dyes such as neutral red (NR, 323.57 mg g^{-1}) and methylene blue (MB, 312.23 mg g^{-1}). The PA adsorbents were also able to remove multiple pollutants successively from water. The adsorption isotherms, kinetics, mechanism, and reusability were also thoroughly investigated. The anionic PVC NPs or dyes were not adsorbed on the surface of the PAs and showed poor adsorption efficiency. The cationic pollutants were removed from water due to strong electrostatic attraction with the negatively charged PA adsorbents. To understand the adsorption mechanism, the adsorption efficiencies of the branched PAs (1–3; A3B2) are compared with linear PAs (4, 5; A2B2) and a model triamide molecule (TA). PA3 showed high adsorption efficiencies compared to other polymers. After extraction of pollutants, all used adsorbents were regenerated using dilute acid washings and reused for pollutant removal from water with a minimum loss of efficiency. As a proof of concept, plastic particles from a commercial facial scrubber were removed efficiently using PA adsorbents. Synthetic functional polymers offer potential solutions for removing emerging pollutants such as plastic micro- and nanoparticles from water.

Received 21st April 2025,
Accepted 31st July 2025

DOI: 10.1039/d5lp00114e

rsc.li/rscapplpolym

Open Access Article. Published on 01 August 2025. Downloaded on 2/5/2026 5:41:45 AM.
This article is licensed under a Creative Commons Attribution-NonCommercial 3.0 Unported Licence.

Introduction

Plastic materials such as polymethylmethacrylate (PMMA), polyvinylchloride (PVC), polyethylene terephthalate (PET), and polystyrene (PS) are widely used in households, industries, and agriculture. Most of the used plastic materials end up in the environment due to poor recycling and improper waste disposal methods. Plastic waste materials undergo slow degradation in the environment and release microparticles (MPs, a size of 5 mm to 1 μm) and nanoparticles (NPs, a size of <1 μm), which cause significant contamination of natural resources.[1–5] Due to their high stability, plastic particles accumulate and contaminate the air, water, and food chain.[6,7] Recent reports have shown that microplastic particles (MPs) and nanoplastic particles (NPs) induce toxicity in living organisms.[8,9] A few methods such as filtration,[10] coprecipitation,[11] and adsorption[12] were used to remove plastic particles from contaminated water samples. Porous materials with large surface areas were used for the adsorption and removal of heavy metal ions and micro- to nanosized plastic particles from water.[13–15] Modified coffee grounds,[16] surface-functionalized cellulose fibers,[12,17] and metal–organic frameworks (MOFs) were also used to remove plastic particles from spiked water samples.[18] However, challenges such as the poor stability of cellulose and the risk of toxic metal leaching from MOFs limit their suitability for large-scale applications.

Synthetic polymers with enhanced pollutant removal efficiencies and environmental stabilities are needed to solve water pollution.[19–22] Recently, Liu *et al.* reviewed the use of three-dimensional covalent organic framework (3D COF) materials prepared from building blocks with different geometries, and diverse geometrical nodes, such as linear, triangular, quadrilateral, tetrahedral, and triangular prism structures.[23] The adopted synthetic route for such 3D materials usually employs interface polymerization.[24,25] In most cases, the reaction between aldehyde and amine functional groups was used to form a rigid imine group as the key step for the formation of a crystalline 3D-framework.[26,27]

Functionalized copolymers are widely used for pollutant removal from water due to their high efficiency and recyclabil-

Department of Chemistry, National University of Singapore, 3 Science Drive 3, Singapore 117543. E-mail: chmsv@nus.edu.sg, e0669547@u.nus.edu

© 2025 The Author(s). Published by the Royal Society of Chemistry

Open Access Article. Published on 01 August 2025. Downloaded on 2/5/2026 5:41:45 AM. This article is licensed under a Creative Commons Attribution-NonCommercial 3.0 Unported Licence.

ity.[28] However, these materials often pose environmental challenges post-usage, as waste membranes exhibit poor degradability. In contrast, aliphatic polyaramides (PAs) are gaining attention as environmentally friendly alternatives, owing to their biodegradable functional groups (*e.g.*, amides). The polyaramides find applications in energy production, storage, 3D printing, and biomedical materials.[29] Recent studies highlight their ability to adsorb heavy metal ions[30–32] and organic pollutants from water,[33,34] making them promising for wastewater treatment. Despite their advantages, a deeper understanding of the adsorption mechanisms and structure–property relationships in synthetic polymers is crucial for optimizing their practical applications.

Here we use a series of highly branched and linear polyaramides (PAs) for water purification. A few important points of our approach include the selected PA networks are insoluble in water and have a branched architecture (A3B2), a large number of surface functional groups, a large surface area, and a strong covalent framework with good chemical, mechanical, and thermal stabilities. Multiple pollutants are used for the adsorption studies to demonstrate the efficiency of the polymers. The current approach employs branched polyaramides (A3B2) with a high density of surface functional groups, resulting in superior adsorption of cationic pollutants as compared to linear polyaramides (A2B2) and small molecular models. By focusing on structural control and tailored functional groups, this design enhances electrostatic interactions for effective removal of pollutants such as microplastics and dyes while maintaining reusability and stability. This method is distinguished by its combination of insolubility, high surface area, and selective adsorption within a polyaramide system. Three structurally different diamines (B2), such as flexible ethylene diamine (EDA), linear rigid *p*-xylene diamine (PXA), and bent *m*-xylene diamine (MXA) were used for the condensation with trifunctional trimesoyl chloride (TMC, A3) or difunctional linear terephthaloyl chloride (TPC, A2) to obtain branched (1–3; A3B2) and linear (4, 5; A2B2) PAs (Scheme 1). A small triamide (TA) molecule was prepared as a model compound to compare the adsorption efficiencies (Scheme 1). Full details of the synthesis, characterization, and applications of PAs 1–5 and TA are discussed along with the adsorption and removal of a few pollutants, such as plastic nanoparticles (*e.g.* PVC NPs), and dissolved dyes, neutral red (NR), and cationic methylene blue (MB) from water. The isotherm and kinetic models were also investigated to understand the adsorption mechanism. The adsorption efficiencies of PAs for multiple pollutants are explained based on the structures and morphologies of the polymer backbone.

Materials and methods

Chemicals and materials

All chemicals were purchased from Sigma-Aldrich with the highest purity (>99%) and used without further purification. Trimesoyl chloride (TMC), ethylenediamine (EDA), triethylamine (TEA), *p*-xylene diamine (PXA), *m*-xylene diamine (MXA), methylene blue (MB), neutral red (NR), cetyltrimethylammonium bromide (CTAB), sodium dodecyl sulfate (SDS), polyvinyl chloride (PVC, MW = ~120 000), and dimethyl formamide (DMF, HPLC grade) were purchased from Sigma-Aldrich Pte. Ltd. The perylene-3,4,9,10-tetracarboxytetrabutylester (PTE) dye was prepared using a previously reported procedure[35] and incorporated inside the polymer NPs for easy tracking.[9] Deionized water was used throughout the experiments.

The FT-IR spectra (500–4000 cm^{-1}) of PAs before and after the polymer nanoparticle (NP) adsorption were recorded using a Bruker ALPHA FT-IR spectrophotometer with KBr as the matrix. A Malvern Zetasizer Nano-ZS90 was used to measure the size and surface charges of the PAs and NPs. A Discovery TGA instrument was used to perform thermogravimetric analysis (TGA) of the samples, which were heated at a rate of 10 °C min^{-1} within the temperature range of 25 °C–1000 °C. A Shimadzu-1601 spectrophotometer was used to record the UV-Vis spectra of each sample. The morphology of the synthesized PVC NPs and PAs was examined using a JEOL JSM-6701F scanning electron microscope (SEM). A Bruker D8 Advance Powder Crystal X-ray diffractometer was used for checking the crystallinity of the materials using Cu Kα radiation (λ = 0.154 nm) within a 2θ range of 5–70° and the source operating at 40 kV and 40 mA. The surface areas of all PA samples were determined using nitrogen sorption experiments using a Quantachrome Autosorb iQ C-XR instrument. The optical images were captured using an EVOS M7000 microscope. Fluorescein isothiocyanate (FITC) and differential interference contrast (DIC) filters were used to acquire the images. The pore size, surface area, and pore volume were measured using N_2 adsorption isotherms at 77 K and 1 atm and analyzed using the Brunauer–Emmett–Teller (BET) method with a Quantachrome Quadrasorb-SI instrument.

Synthesis of PAs from trimesoyl chloride (A3) and diamines (B2)

Highly branched PAs 1–3 were synthesized using trifunctional trimesoyl chloride (TMC, A3) and different difunctional diamines (B2) such as ethylenediamine (EDA, PA1), *p*-xylene diamine (PXA, PA2) and *m*-xylene diamine (MXA, PA3), respectively, under ambient conditions.[36,37] In a typical procedure, TMC (0.5 g, 1.88 mmol) was dissolved in dimethylformamide (DMF, 50 mL) and cooled to 0 °C. To this solution, a mixture of triethylamine (2 mL) and the appropriate diamine (*e.g.* EDA or PXA or MXA, 2.8 mmol, 1.5 equiv.) dissolved in DMF (10 mL) was added dropwise within 30 minutes at 0 °C. The solution was stirred at 0 °C for 30 minutes and warmed to room temperature overnight. The white solid product obtained was filtered and rinsed with excess DMF, followed by water to remove all soluble impurities. The white solid was dried in an oven at 65 °C for 24 h and used for further characterization. Surface area and porosity measurements were conducted using a Quantachrome Quadrasorb-SI analyzer. For nitrogen (N_2), measurements were taken at 77 K and 1 atm, while for carbon dioxide (CO_2), they were performed at 273 K and 1 atm. The

Open Access Article. Published on 01 August 2025. Downloaded on 2/5/2026 5:41:45 AM.
This article is licensed under a Creative Commons Attribution-NonCommercial 3.0 Unported Licence.

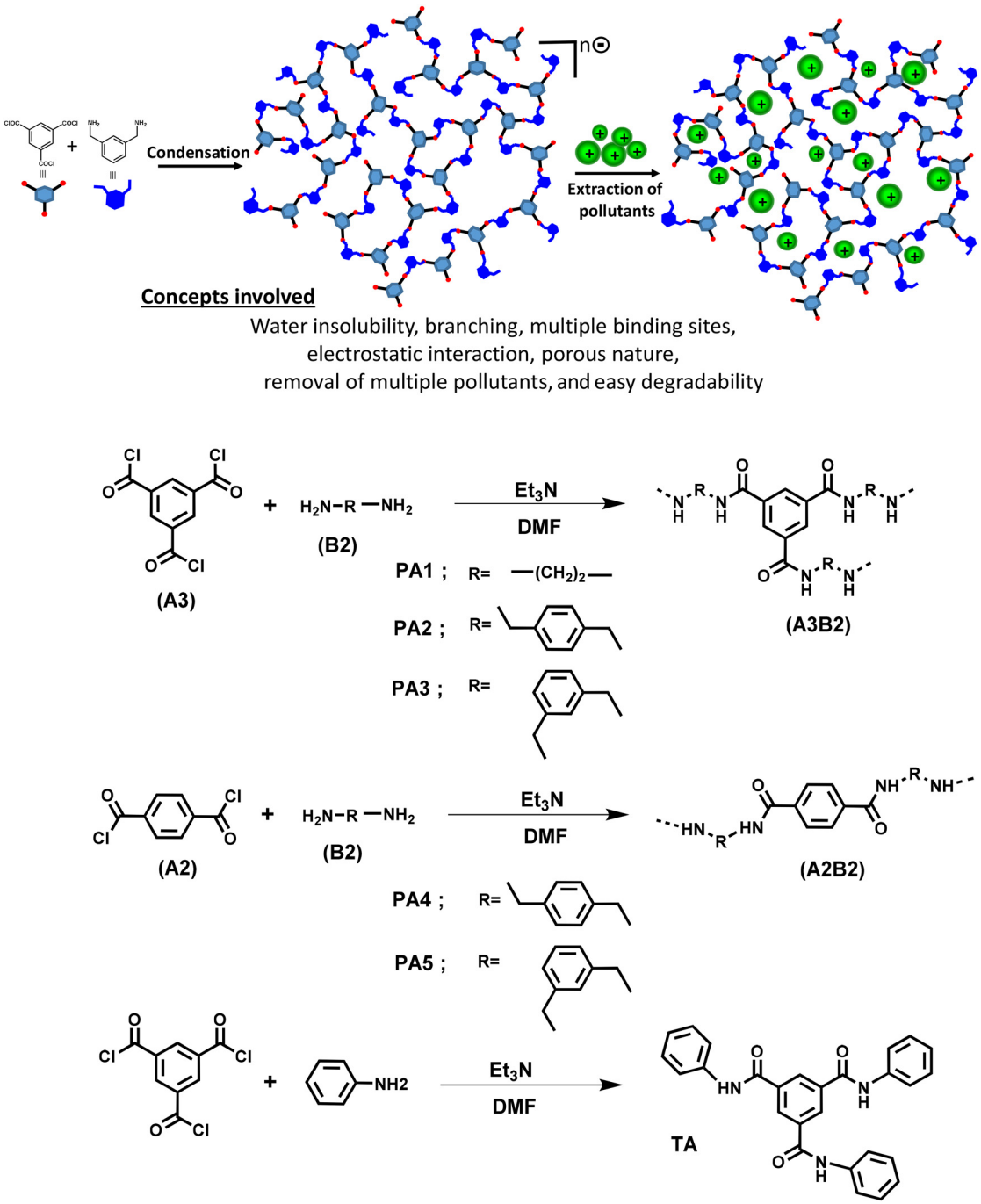

Scheme 1 Synthesis route to PAs 1–5 and TA.

surface areas, pore diameters, and pore volumes were calculated from the collected isotherm data using the Brunauer–Emmett–Teller (BET) method. The data are plotted and provided in the SI.

Synthesis of linear PA from terephthaloyl chloride (A2) and diamines (B2)

Bifunctional terephthaloyl chloride (TPC, 0.5 g, 2.43 mmol) was reacted with MXA or PXA (2.46 mmol, 1 equiv.) to obtain linear polymers PA4 and PA5, respectively.[38] All other experimental conditions mentioned above were kept the same for synthesizing linear polyaramides PA4 and 5. The white solids obtained were dried at 65 °C and used for further characterization and adsorption of pollutants from water.

Synthesis of triamide (TA)

Trimesoyl chloride (TMC, 0.5 g, 1.88 mmol) was dissolved in DMF (50 ml), and TEA (1 ml, excess) was added along with an

© 2025 The Author(s). Published by the Royal Society of Chemistry

Open Access Article. Published on 01 August 2025. Downloaded on 2/5/2026 5:41:45 AM. This article is licensed under a Creative Commons Attribution-NonCommercial 3.0 Unported Licence.

appropriate quantity of aniline (6.59 mmol, 3.5 equiv.). The reaction was conducted under conditions similar to those reported in the literature.[39] The TA formed was precipitated from water (200 ml) to obtain a white solid, which was filtered, washed multiple times with water, and dried in an oven at 65 °C, which was used for further characterization. The resultant TA was used for the adsorption of pollutants, and the results are compared with that of polymers.

Preparation of cationic and anionic PVC nanoparticles (PVC NPs)

PVC NPs encapsulated with the PTE dye were synthesized and fully characterized to evaluate the effectiveness of polyaramide networks for the adsorption of such plastic particles from water.[35,40] PVC NPs were synthesized using commercially available PVC (250 mg, MW-120 000), PTE (12.5 mg, 5 wt% of polymer), and CTAB for cationic or SDS for the anionic surfactant (10 mg, 4 wt% of polymer), which were taken in a standard flask (50 mL). An optically active PTE dye was used to monitor and calculate the removal efficiency of PAs. The mixture was dissolved in THF (100 mL) through sonication. A portion (5 mL) of the polymer stock solution in THF was poured into deionized water (50 mL) and stirred continuously overnight to form monodispersed particles and to remove traces of the organic solvent THF *via* slow evaporation. The clear solution obtained was filtered through a cotton plug to remove undissolved or large plastic debris. PVC NPs stabilized with CTAB are indicated as (+) PVC NPs, and SDS-incorporated particles as (−) PVC NPs. Finally, UV-Vis spectroscopy, fluorescence spectroscopy, dynamic light scattering (DLS), and scanning electron microscopy were used to characterize the NPs. The aqueous stock solutions of both NPs were stored at room temperature in a glass bottle for adsorption experiments.

Extraction of NPs, NR, and MB dyes from water using PAs

The batch adsorption studies were carried out by mixing appropriate PAs (25 mg) with (+) PVC NP solution at different concentrations (6 mL, 5–150 mg L^{-1}) and shaking the mixture on a mechanical shaker at various time points (15 min–300 min). The mixture was centrifuged, and the supernatant was removed and analyzed using UV-Vis spectroscopy to estimate the amount of plastic particles left in the solution. This was followed by calculating the removal efficiency and adsorption capacity of (+) PVC NPs. All experiments were done in three replicates and the average value is given here.

Similarly, separate batch experiments were performed to examine the adsorption of the molecular dyes MB and NR on PAs. In a batch experiment, an appropriate PA (25 mg) was added to the dye solution (6 mL, 50 mg L^{-1}), and the mixture was continuously stirred at 350 rpm. The effects of variables such as contact time and concentrations were carefully examined. The adsorption data of dyes (MB and NR) at various starting concentrations (5–150 mg L^{-1}) and fixed concentrations of the appropriate PAs were used to check the best isotherm models, such as Langmuir and Freundlich isotherms.[11,41] To determine the various kinetic parameters, the adsorption of dyes (MB and NR) on the PA surface from solutions at different time intervals was measured using UV-Vis spectroscopy. All adsorption experiments were performed three times at a neutral pH of 7, and the average value was reported. The percentage removal efficiency of added pollutants (*i.e.* (+) PVC NPs, NR, and MB) by PAs was calculated using eqn (1).[41]

$$\text{Removal efficiency}\,(\%) = \left[\frac{C_0 - C_f}{C_0}\right] \times 100\% \quad (1)$$

where C_0 and C_f are the initial and the equilibrium concentrations of analytes in mg L^{-1}.

The adsorption efficiency at equilibrium (Q_e, mg g^{-1}) was calculated using eqn (2),

$$Q_e = \frac{[(C_0 - C_e) \times V]}{W} \quad (2)$$

where V is the volume of the adsorbate solution (L) and W is the mass (g) of the PAs used.

Adsorption and kinetic studies

Batch adsorption was used to obtain data for mechanistic studies using different kinetic and isotherm models. Individual PAs (25 mg) were mixed with three positively charged adsorbate ((+)PVC NPs, NR, and MB) solutions (6 mL, 50 mg L^{-1}) at room temperature and shaken for different time points (15 min–300 min) using a mechanical shaker. The solutions were allowed to settle for 3 min and centrifuged, and the supernatant was examined for the remaining adsorbent using UV-Vis spectroscopy to determine the removal efficiency. For each set of conditions (*e.g.* concentration of PAs and pollutants), triplicate experiments were carried out at a neutral pH of 7, and the average value was reported. Pseudo-first-order and pseudo-second-order kinetic models were used to study the adsorption kinetics of PAs with the analytes. Eqn (3) and (4) represent the linear form of pseudo-first-order and pseudo-second-order kinetic models.[42]

$$\ln(Q_e - Q_t) = \ln(Q_e) - k_1 t \quad (3)$$

$$\frac{t}{Q_t} = \frac{t}{Q_e} + \frac{1}{k_2 Q_e^2} \quad (4)$$

where Q_t (mg g^{-1}) indicates the adsorption capacity at time t, Q_e (mg g^{-1}) refers to the adsorption capacity at equilibrium, and k_1 is the pseudo-first-order rate constant (min^{-1}). Based on the slope and intercept of the linear curves, the k_1 and k_2 values and the adsorption capacities were determined.

Isotherm analysis

An appropriate amount of PA or TA adsorbent (25 mg) was dispersed in adsorbate (PVC NPs, NR, and MB) solutions (6 mL) at different concentrations (5–150 mg L^{-1}) and used for the adsorption isotherm studies at room temperature. The adsorption experiments were conducted three times at each concentration and a neutral pH of 7, and average values were reported. The data were analyzed using both Langmuir[43,44] and Freundlich[30] isotherm models.

Open Access Article. Published on 01 August 2025. Downloaded on 2/5/2026 5:41:45 AM.
This article is licensed under a Creative Commons Attribution-NonCommercial 3.0 Unported Licence.

The Langmuir adsorption isotherm is represented by eqn (5),[41]

$$\frac{C_e}{Q_e} = \frac{C_e}{Q_m} + \frac{1}{K_L Q_m} \quad (5)$$

where C_e (mg L^{-1}) represents the equilibrium concentration of the adsorbate, Q_e (mg g^{-1}) is the equilibrium adsorption capacity, K_L (L mg^{-1}) is the Langmuir adsorption equilibrium constant, and Q_m (mg g^{-1}) is the maximum adsorption capacity.

The Freundlich adsorption isotherm is expressed by the following formula (eqn (6)).[41,45]

$$\log q_e = \frac{1}{n}\log c_e + \log k_F \quad (6)$$

where c_e is the concentration of the adsorbate (mg L^{-1}), n is the empirical parameter, and k_F (L mg^{-1}) is the Freundlich constant.

Effect of pH on adsorption

The changes in the pH of the solution usually show a significant impact on the removal rate. The study was done at pH = 2 (acid medium), pH = 7 (neutral medium), and pH = 11 (basic medium). Aqueous solutions of HCl and NaOH (0.1 M) were used to adjust the pH of (+)PVC NPs, NR, and MB solutions to 2 and 11, respectively. Extreme care was taken to avoid any precipitation or changes in the spectroscopic behavior of the dyes at various pH values used. The other parameters such as contact time (2 h), adsorbent dosage (25 mg), pollutant concentration (50 mg L^{-1}) and agitation speed (350 rpm) were maintained constant. All experiments were conducted three times, and average values were reported.

Successive adsorption and removal of multiple pollutants

The studies reported in the literature include one specific adsorbent used for removing a pollutant from water. However, common environmental samples are contaminated with multiple pollutants, and therefore, it is important to explore how a few pollutants are removed using a single adsorbent. Here an appropriate amount (25 mg) of PAs 1–3 was used for the adsorption of multiple pollutants successively at a neutral pH of 7. Positively charged PVC NP solution (6 mL, 50 mg L^{-1}) was added to the PA, shaken for 2 h, centrifuged, and both the supernatant and solid adsorbent were collected. The supernatant was analyzed using UV-Vis spectroscopy to monitor the adsorption. The collected solid PAs with (+)PVC NPs adsorbed on the surface were denoted as PA1/(+)PVC NPs, PA2/(+)PVC NPs, and PA3/(+)PVC NPs. The zeta potentials of the PAs after adsorption of (+)PVC NPs were measured, filtered, dried at 65 °C for 12 h, and reused for adsorption of negatively charged (−)PVC NPs, followed by cationic dye MB from solution using the same procedure described above. Thus, successive adsorption of positively charged (+)PVC NPs, negatively charged (−)PVC NPs, and cationic MB dye was done to check on the removal efficiencies of the adsorbent toward pollutants. The main driving force for such adsorption is the changes in surface potential (*i.e.* PA/(+)PVC NPs/(−)PVC NPs/(+)MB) with the alternate adsorption of oppositely charged pollutants. All experiments were conducted three times at a neutral pH of 7, and average values were reported.

Regeneration studies

The PA adsorbents with pollutant molecules on the surface were rinsed with a dilute HCl solution (0.3 M, 10 mL) and washed with water multiple times to eliminate any remaining acid on the surface. PAs are stable in dilute acid as compared to a basic medium. The washed solid PAs were dried at 65 °C and used for the adsorption of pollutants ((+)PVC NPs, NR, and MB) from water. Five repeated trials of washing and regeneration of adsorbents showed effective adsorption of pollutants with no significant loss in adsorption efficiencies.

Removal of polymer nanoparticles from a commercial facial scrub using PAs

The plastic particle removal efficiency of PAs was tested using a commercial facial scrub purchased from a local shop. A fixed amount of the facial scrub was dried slowly at room temperature to remove the water content and the obtained white powder was used for preparing a stock solution for further experiments. In a typical procedure, appropriate amounts of PAs (25 mg) were mixed with diluted scrubber solution (6 ml, 50 mg L^{-1}) and kept on a mechanical shaker for a 2 or 5 h period. After shaking, the mixture was centrifuged, and the supernatant was analysed using UV-Vis spectroscopy. All experiments were conducted three times at a neutral pH of 7, and average values were reported. The adsorption efficiency was calculated from the absorbance data and the solid PA adsorbed with the plastic particles from the scrubber was characterized using a range of techniques.

Results and discussion

Preparation and characterization of PAs and NPs

All PAs were prepared using the reaction between TMC and three diamines EDA (PA1), PXA (PA2), and MXA (PA3) *via* a standard procedure.[26,30] The FTIR spectra of the PAs showed a peak at 3088 cm^{-1}, which is due to aromatic –C–H bonds on the polymer backbone. The peaks from aliphatic CH_2 groups on the polymer backbone of PA were observed at 2853 and 2943 cm^{-1}.[46] The starting material TMC (Fig. 1a,i) showed a peak at 1743 cm^{-1}, which corresponds to the absorption peak of >C═O of the acid chloride group, which is not present in the spectra of all PAs (Fig. 1a,i).[37,46] The FTIR spectra of PAs showed peaks at 1660 cm^{-1} and 1542 cm^{-1}, which correspond to >C═O of the amide I and amide II peaks, respectively (Fig. 1a,ii–iv).[47] The broad peak located at 3400 cm^{-1} is due to the stretching vibration of the N–H groups of the amide on the PA backbone.[48] Similar peaks are also observed in the FTIR spectra of PAs 4, 5 and TA (Fig. S1a).

As-synthesised PA1 and PA3 showed single broad XRD peaks around 25.49° (3.49 Å) and 24.77° (3.59 Å), respectively, which showed amorphous lattices (Fig. 1b,i and iii).[46] This could be accounted for by the flexible ethyl spacer of PA1 and the kink

© 2025 The Author(s). Published by the Royal Society of Chemistry

Open Access Article. Published on 01 August 2025. Downloaded on 2/5/2026 5:41:45 AM.
This article is licensed under a Creative Commons Attribution-NonCommercial 3.0 Unported Licence.

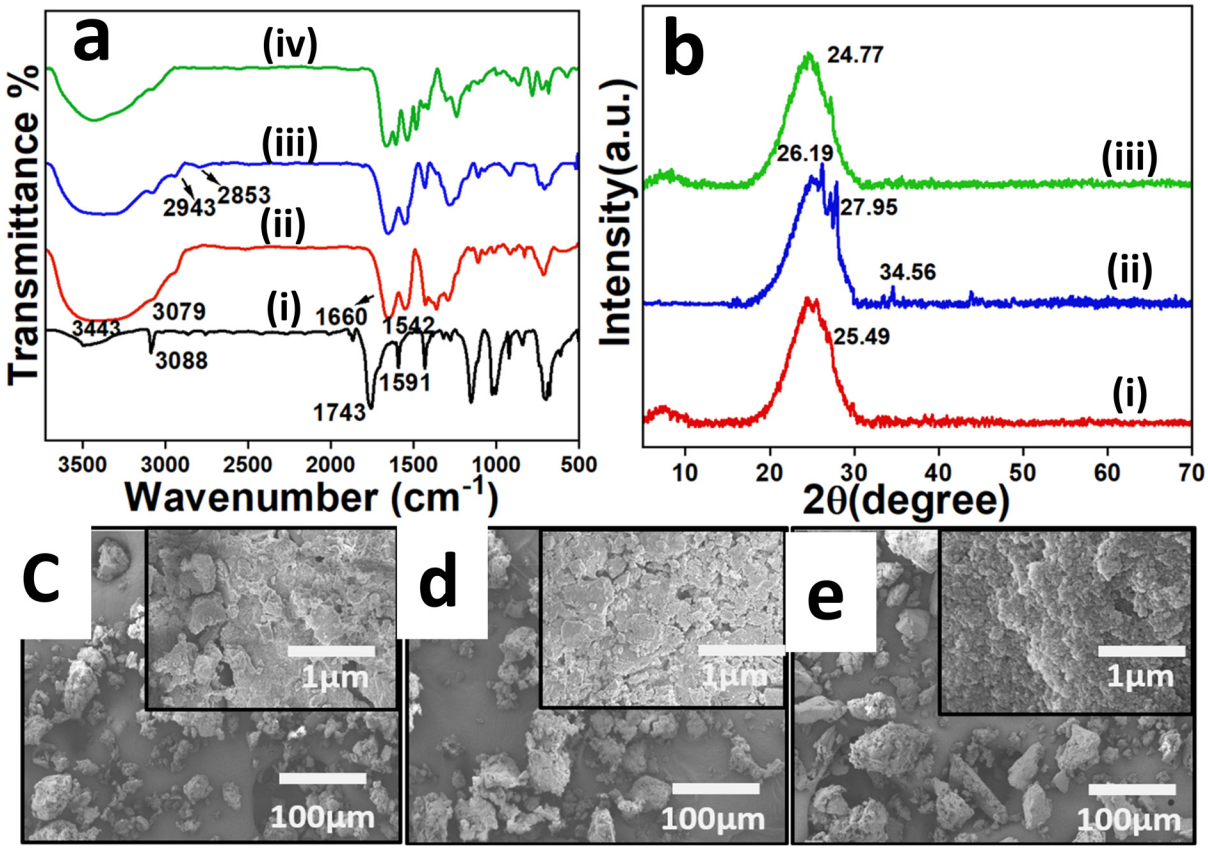

Fig. 1 FTIR spectra (a, i–iv) and XRD patterns (b, i –iii) of as-synthesised PA1 (—), PA2 (—), and PA3 (—). The FITR spectrum (a, i) of the starting material TMC is given for comparison. SEM micrographs of synthesised PA1 (c), PA2 (d), and PA3 (e). Similar micrographs for PA4, 5 and TA are given in the SI (Fig. S1).

nature of the MXA in PA3, which distorts the packing of the chains inside the lattice. The broad peaks focused around 2θ = 25° imply a disordered lattice with long-range H-bonds inside the lattice. The XRD of PA2 showed sharp, intense peaks at 26.19° (3.39 Å), 27.95° (3.18 Å), and 34.56° (2.59 Å) (Fig. 1b,ii), which implies a crystalline lattice for PA2. The absence of peaks in the low 2θ region in the XRD diffraction pattern implies no long-range order inside the lattice. The linear PXA for preparing PA2 offers a rigid but branched 2D architecture with strong interlayer short-range H-bonds. The XRD patterns of PAs 4, 5, and TA are given in Fig. S1b, i–iii. The broad peak appeared at 24.49 (3.64 Å), indicating that PA4 has an amorphous character. Sharp peaks appeared at 2θ = 18.56° (4.78 Å), 21.55° (4.13 Å), and 28.09° (3.17 Å) for PA5, indicating a semicrystalline nature. These two PA architectures are linear and able to interact strongly with neighboring polymer chains through long-range intra-and interchain H-bonds. As expected, the TA showed sharp peaks at 2θ = 12.64° (6.99 Å), 31.80° (2.810 Å), and 38.59° (2.33 Å), representing a crystalline lattice.[49] This is due to the strong intermolecular H-bond assisted self-assembly. The surface properties and structure of the polyaramides were established using dynamic light scattering and gas adsorption measurements.

The optical properties and surface morphologies of the prepared (+)PVC NPs were characterised using DLS, SEM, UV-Vis, and fluorescence spectroscopy (Fig. 2). The SEM images of all synthesised PAs showed particles with irregular shapes (Fig. 1c–e and S1c, d), and TA showed a flake-type morphology (Fig. S1e). TGA results indicate that the prepared samples showed the high thermal stability of typical polyaramides with initial thermal degradation starting at 350–420 °C (Fig. S2). The TGA traces showed a mass loss of 60.5 ± 0.1%, 71.3 ± 0.6%, 72.4 ± 1.3%, 65.5 ± 0.3%, 72.2 ± 1.2%, and 88.6 ± 0.9%, for PAs 1–5 and TA, respectively, above 350 °C–1000 °C (Fig. S2a and b).

The surface charges of the particles originated from the type of surfactant used for the stabilization with CTAB-incorporated particles showing a positive value and SDS-stabilised one with negative values. The (+)PVC NPs and (−)PVC NPs showed +22.14 ± 1.44 and −32.04 ± 0.97 zeta potential values, respectively. The hydrodynamic size of (+)PVC NPs was observed as 133.23 ± 2.56 nm, and that of (−)PVC NPs was 144.63 ± 1.45 nm. The SEM images of the (+)PVC NPs (Fig. 2a) and (−)PVC NPs (Fig. S3) showed spherical particles with an average dry size of 120.12 ± 0.45 nm and 135.33 ± 1.40 nm with a relatively narrow size distribution (Fig. 2a, inset). Such

© 2025 The Author(s). Published by the Royal Society of Chemistry

Open Access Article. Published on 01 August 2025. Downloaded on 2/5/2026 5:41:45 AM.
This article is licensed under a Creative Commons Attribution-NonCommercial 3.0 Unported Licence.

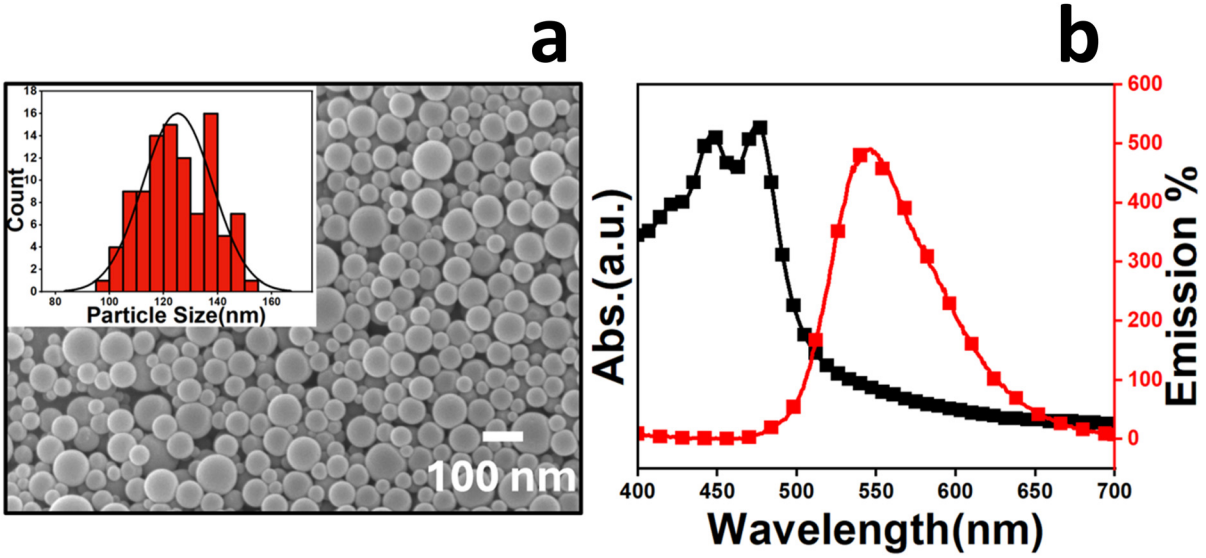

Fig. 2 SEM image of dry (a) and absorption and emission spectra (b) of water dispersion of (+)PVC NPs. The inset in (a) represents the size distribution of the particles calculated from SEM images. The SEM image of (−)PVC NPs is given in Fig. S3.

size differences are expected due to the different types (dry for SEM and water dispersion for DLS) of PVC NPs used in measurements. The UV-Vis spectra (Fig. 2b) of the particles showed absorbance peaks at 440 nm and 470 nm and the emission spectrum with a peak at 550 nm, corresponding to the PTE dye encapsulated inside the particles.

Effect of the concentration of PAs on adsorption

To monitor the adsorption of the cationic PVC NPs, and dyes, NR and MB, the UV-Vis spectra of the supernatant solutions were recorded before and after adsorption on PAs (Fig. 3a–c).

The optical images of the solutions before (i) and after (ii) adsorption on PAs are shown along with the absorption spectra (Fig. 3, inset). The yellow colour of the (+)PVC NP solution was changed to colourless after the adsorption experiment. A comparison of the UV-Vis spectra of solutions before and after the adsorption experiments revealed that absorbance peaks from (+)PVC NPs, NR, and MB were fully eliminated from the supernatant liquid after shaking with PAs (Fig. 3a, c and e), implying complete adsorption and removal of the particles and dyes from solution. Increased adsorbent dosage resulted in enhanced removal effectiveness of NPs within 2 h (Fig. 3d). At a maximum concentration (25 mg) of PAs and an adsorption time of 2 h, removal efficiencies were increased to 94.1 ± 1.5% (PA1), 89.3 ± 0.5% (PA2) and 99.7 ± 0.03% (PA3). The linear polyaramides PA4 and PA5 showed removal efficiencies in the range of 72–76% for PVC NPs (Fig. S4a) and MB (Fig. S4b). Similarly, the TA showed ~70% removal efficiencies for the pollutants examined (Fig. S4c). The strong electrostatic interactions between the negatively charged PAs and the positively charged PVC NPs, and cationic MB enhanced the removal efficiencies. At the same time, the molecular structure of the polyaramides and surface charges are responsible for the observed differences in removal efficiencies. High efficiencies are expected for the network structure of PAs 1–3, which helps to trap the pollutants inside the cavities of polymer lattices. Since linear PAs (PAs 4, 5) and TA showed lower removal efficiencies, further mechanistic studies were focused only on the branched PAs 1–3. The UV-Vis spectra of pristine PVC NPs without adding any PAs before and after centrifugation are given in the SI (Fig. S5), indicating that the PVC NPs were not affected by the centrifugation process.

Effect of the time and concentration of PVC NPs, MB, and NR on absorption capacity

The effect of experimental parameters such as time and concentrations of (+)PVC NPs and MB dye on the removal efficiency of PAs was tested (Fig. 4). The time-dependent extractions were done during a period of 0–300 min using a fixed amount of PAs (25 mg) and a fixed concentration of the pollutants of 50 mg L^{-1}. The pollutant solution at different concentrations (0–150 mg L^{-1}) and fixed amounts of PAs (25 mg) were used for adsorption at a time duration of 120 minutes. The changes in the removal efficiencies of PAs concerning time and concentrations of the pollutants are shown in Fig. 4.

The equilibrium was obtained after 200 minutes and the removal efficiency of PA1 increased with time and reached 80.7 ± 0.02% ((+)PVC NPs), 92.8 ± 0.87% (NR), and 82.81 ± 0.82% (MB) after 300 min (Fig. 4a and b). For PA1, the removal rate was decreased with an increase in the concentrations of pollutants, (+)PVC NPs, NR, and MB (Fig. 4b). PA1 (25 mg) showed a higher removal efficiency of 84 ± 0.9% for PVC NPs, 85.9 ± 1.3% for NR, and 87.1 ± 1.8% for MB at a low concentration of 5 mg L^{-1} (Fig. 4b). At a high concentration of the pollutants (150 mg L^{-1}), the removal efficiencies were decreased to 17.1 ± 1.9, 21.1 ± 3.2, and 42.2 ± 4.3% for (+)PVC NPs, NR, and MB, respectively. Since the removal of pollutants is based on surface adsorption, this is expected due to the saturation of the PA surface with the pollutants.

© 2025 The Author(s). Published by the Royal Society of Chemistry

Open Access Article. Published on 01 August 2025. Downloaded on 2/5/2026 5:41:45 AM.
This article is licensed under a Creative Commons Attribution-NonCommercial 3.0 Unported Licence.

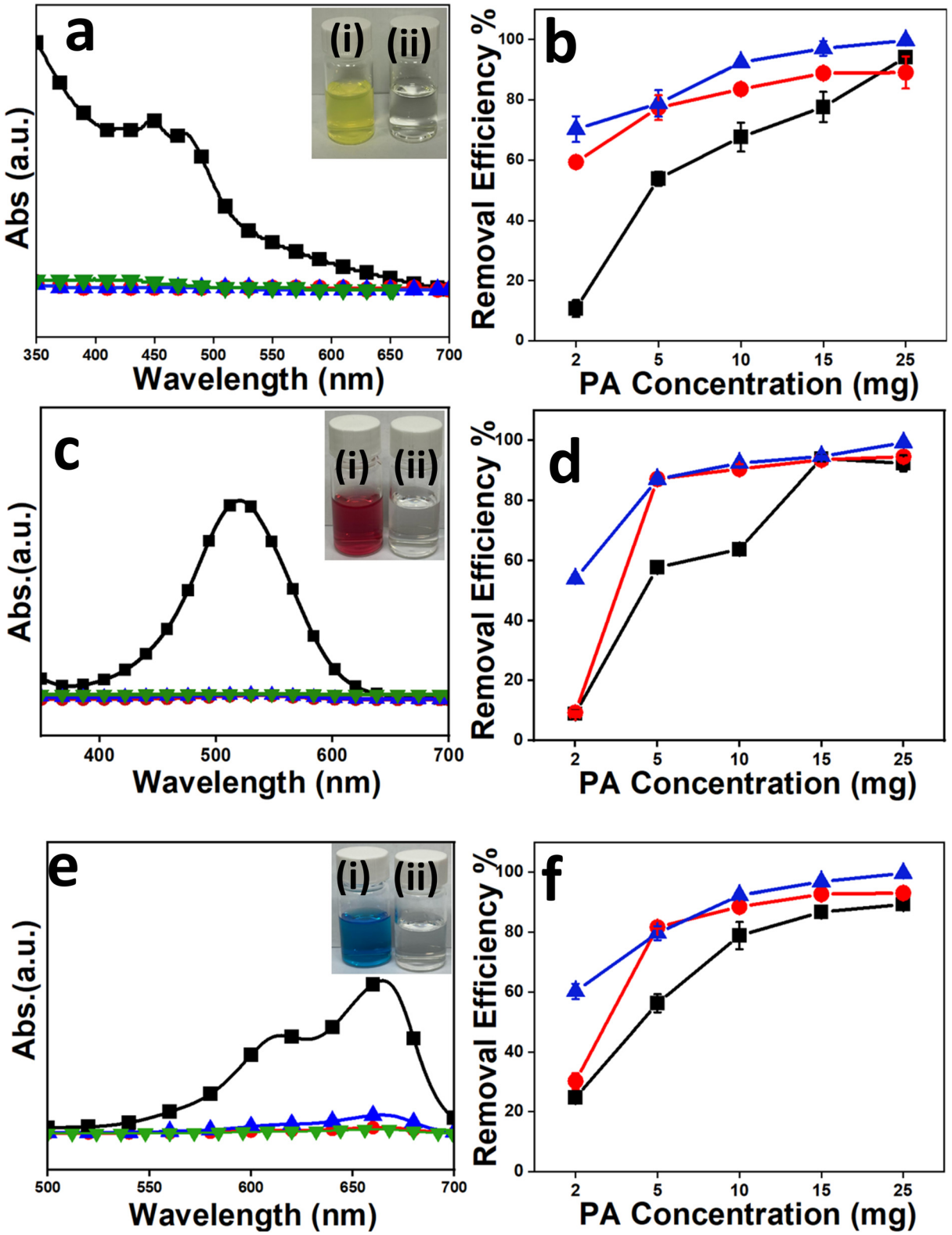

Fig. 3 Absorbance spectra of the solution before (-■-) and after adsorption on PA1 (-●-), PA2 (-▲-), and PA3 (-▼-) for the removal of PVC NPs (a), NR (c), and MB (e) and the calculated removal efficiencies of PA1 (-■-), PA2 (-●-), and PA3 (-▲-) for PVC NPs (b), NR (d), and MB (f). The concentration of the pollutants was kept constant as 50 mg mL^{-1}. The inset shows the optical images of solutions before (i) and after (ii) adsorption, indicating the complete removal of PVC NPs, NR, and MB. The removal efficiencies of PA4, PA5, and TA with changes in the concentration of PAs are given in the SI (Fig. S4).

© 2025 The Author(s). Published by the Royal Society of Chemistry

Open Access Article. Published on 01 August 2025. Downloaded on 2/5/2026 5:41:45 AM.
This article is licensed under a Creative Commons Attribution-NonCommercial 3.0 Unported Licence.

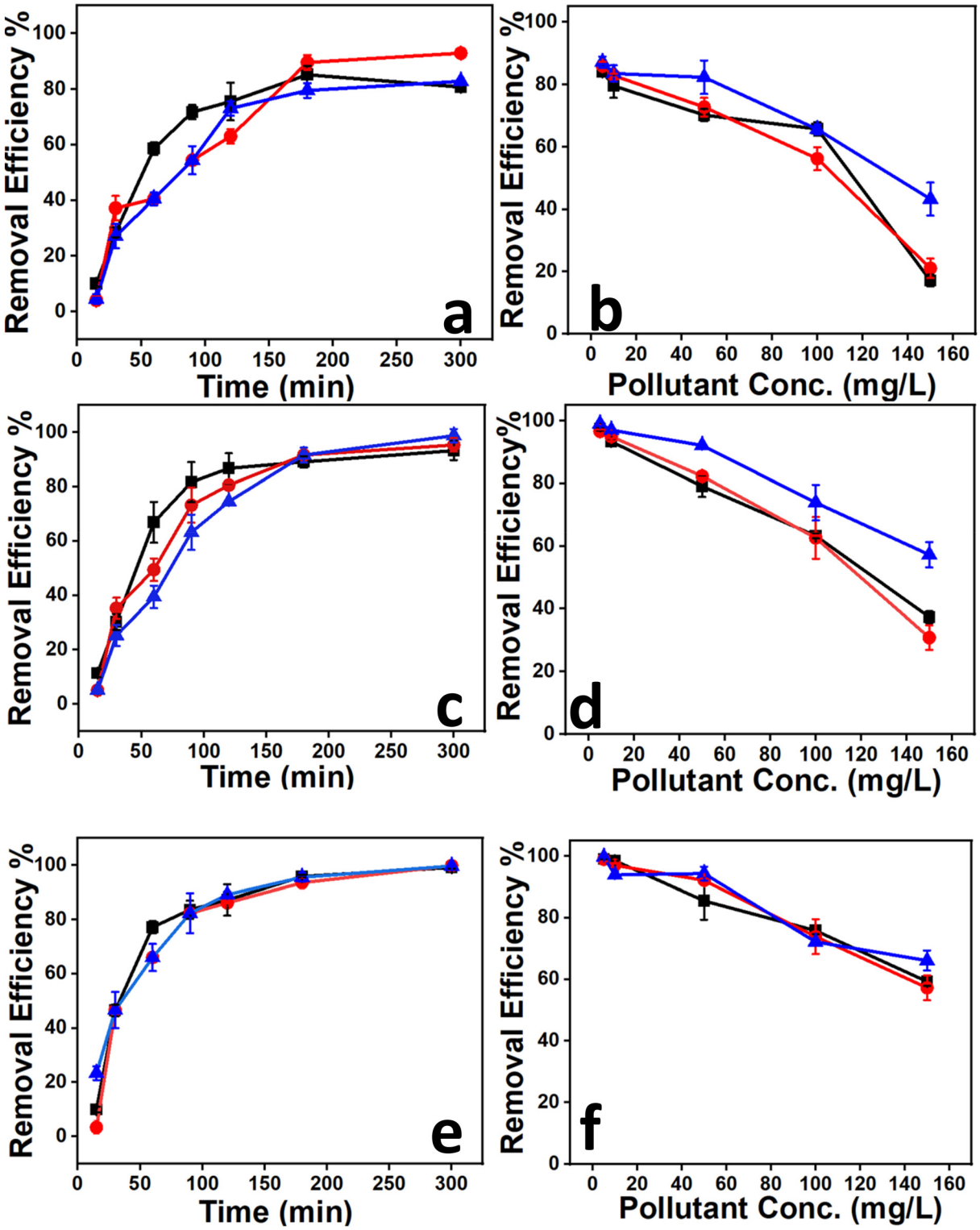

Fig. 4 Effect of time (0–300 min, a, c and e) and concentration (0–150 mg L^{-1}, b, d and f) of -■- (+)PVC NPs, -●-NR and -▲-MB on removal efficiencies – PA1 (a and b), PA2 (c and d) and PA3 (e and f). The amount of all PAs used for the adsorption experiments was kept constant as 25 mg. For time dependent studies, the concentration of the pollutants was fixed at 50 mg L^{-1}. The data for PA3, PA4, and TA are given in Fig. S6.

Similarly, after 200 minutes, the system reaches equilibrium and the removal efficiency of PA2 rose to 82.8 ± 3.5% for MB, 92.8 ± 2.45% for NR, and 80.7 ± 2.3% for (+)PVC NPs at a concentration of 5 mg L^{-1} of the pollutants (Fig. 4c and d). When a high concentration (*i.e.* 150 mg L^{-1}) of the pollutants was used (Fig. 4d), the removal efficiencies of PA2 decreased to

© 2025 The Author(s). Published by the Royal Society of Chemistry

Open Access Article. Published on 01 August 2025. Downloaded on 2/5/2026 5:41:45 AM. This article is licensed under a Creative Commons Attribution-NonCommercial 3.0 Unported Licence.

37.4 ± 1.8% for (+)PVC NPs, 30.8 ± 3.9% for NR, and 57.2 ± 4.1% for MB.

Similarly, the removal efficiency was increased to 99.1 ± 0.5% for (+)PVC NPs, 99.8 ± 0.06% for NR, and 99.7 ± 0.2% for MB after 300 min (Fig. 4e). PA3 showed removal efficiencies of 99 ± 0.4%, 98.97 ± 0.7%, and 99.7 ± 0.1% for a low concentration (5 mg L^{-1}) of pollutants, which decreased to 59.2 ± 1.4%, 57.2 ± 4.1%, and 66.1 ± 3.3% at a high concentration of 150 mg L^{-1} (Fig. 4f). This is expected due to the saturation of the surface of PAs with the concentration-dependent adsorption of pollutants. For PA4, PA5, and TA, the adsorption equilibrium was achieved after 120 min (Fig. S6a, c and e). Similarly, all three adsorbents showed high removal efficiencies for (+)PVC NPs. As stated above for PA1–3, the PA4, PA5, and TA showed similar concentration-dependent behaviour of the pollutants towards removal efficiencies. The removal efficiencies decreased with an increase in the concentration of pollutants.

Characterization of PAs after adsorption

The FTIR spectra (Fig. S7a–c) and TGA traces (Fig. S8a–c) of PAs after adsorption of the pollutants did not show significant changes. This is due to the relatively low amount of pollutants adsorbed on the PA surface as compared to the bulk. The FTIR spectrum of pristine PVC NPs showed peaks at 614 cm^{-1} (–C–Cl bending vibration), 959 cm^{-1} (C–H wagging), 1254 cm^{-1} (C–H rocking), 1425 cm^{-1} (CH_2 deformation), and a sharp peak at 2943 cm^{-1} and 2853 cm^{-1} (CH_2-stretching) (Fig. S7a,i).[12]

The FTIR spectra after adsorption of (+)PVC NPs (Fig. S7a, ii–iv) showed the corresponding spectra of PAs. FTIR spectra after adsorption of other dyes (NR and MB) also showed similar spectra of PAs (Fig. S7b and c). The peaks appeared at 1242 cm^{-1} (C=C stretching vibration) for the PAs are visible in all FTIR spectra, and the peak at 1324 cm^{-1} (C–N stretching vibration) of the dyes was not observed in the FTIR spectra of polymers after adsorption. The dyes (NR and MB) also showed strong C–H absorption peaks at 2943 cm^{-1} and 2853 cm^{-1}, which were not visible in the case of PAs. TGA of all three PAs after adsorption of pollutants was done under a N_2 atmosphere using a heating rate of 10 °C per minute from room temperature to 1000 °C (Fig. S8). The initial weight loss (<10%) observed below 200 °C is usually due to the loss of solvent molecules entrapped inside the polymer lattice. The second weight loss around 350 °C indicates the degradation of the polymer backbone.

SEM images of PAs after adsorption of (+)PVC NPs showed the presence of spherical particles on the surface (Fig. 5a–c). Such particles are part of the PAs and are not from the pollutants. The adsorbed dye molecules are not visible in SEM; however, the optical images of PAs after adsorption of dyes showed blue emission in the DAPI mode and red emission in the Texas Red mode, which confirms the presence of MB and NR on the PA surface (Fig. 6). The green fluorescence images of the (+)PVC NPs adsorbed PAs are given in Fig. S9.

Isotherm model studies

To understand the mechanism of adsorption of pollutants on the surface of PAs, the adsorption isotherm models are used to fit the data. Popular isotherm models such as the Langmuir and Freundlich models are used to establish the mechanism. The homogeneous monolayer formation of adsorbate molecules on the surface of the PA adsorbent with a finite number of similar and equivalent adsorption sites is explained by the Langmuir isotherm model. On the other hand, the Freundlich isotherm model uses multilayer adsorption on the PA surface that isn't uniform and has a multilayer distribution of active sites.[50]

The PAs (25 mg) were mixed with one of the pollutants, *i.e.* (+)PVC NPs, NR, and MB, at varying concentrations (0, 5, 25, 50, 100, and 150 mg L^{-1}) and stirred mechanically for 2 h. The supernatant was collected after 2 h and used to calculate the remaining amounts of adsorbate in the solution by measuring the absorbance. Langmuir and the Freundlich isotherm models were used to analyze the data (Fig. 7a–f, Fig. S10a–f and Table 1). The equations related to the Langmuir and Freundlich isotherm models are given in the Materials and methods section (eqn (5) and (6)). The correlation of Q_e *vs.* C_e was plotted to examine the relevance of the equilibrium data of pollutants, which fits well with the Langmuir model for both (+)PVC NPs and dyes (NR, and MB).

For all PAs, the Langmuir model showed higher R^2 values for the data collected for PVC NPs, NR, and MB as compared to the Freundlich model. The SI (Fig. S10) provides a Freundlich isotherm model analysis of the data obtained from the adsorption. In Fig. 7e (Table 1), PA3 showed high Q_{max} values of 83.33, 95.06, and 157.75 mg g^{-1} for PVC NPs, NR,

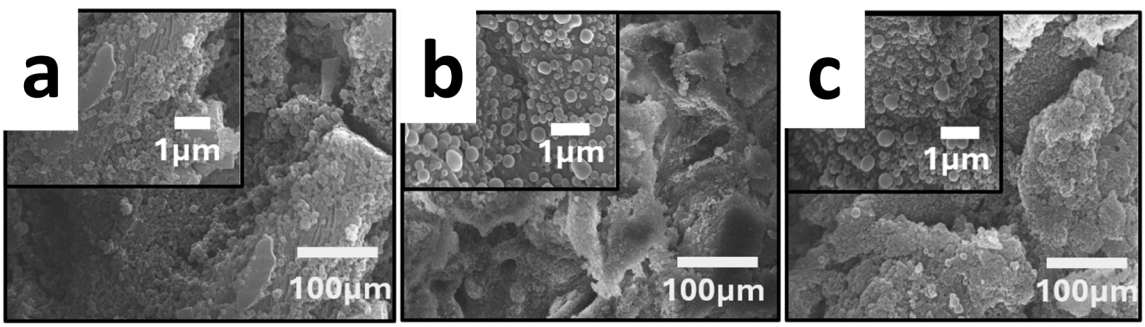

Fig. 5 SEM images of PA1 (a), PA2 (b), and PA3 (c) after adsorption of (+)PVC NPs from the solution.

© 2025 The Author(s). Published by the Royal Society of Chemistry

Open Access Article. Published on 01 August 2025. Downloaded on 2/5/2026 5:41:45 AM.
This article is licensed under a Creative Commons Attribution-NonCommercial 3.0 Unported Licence.

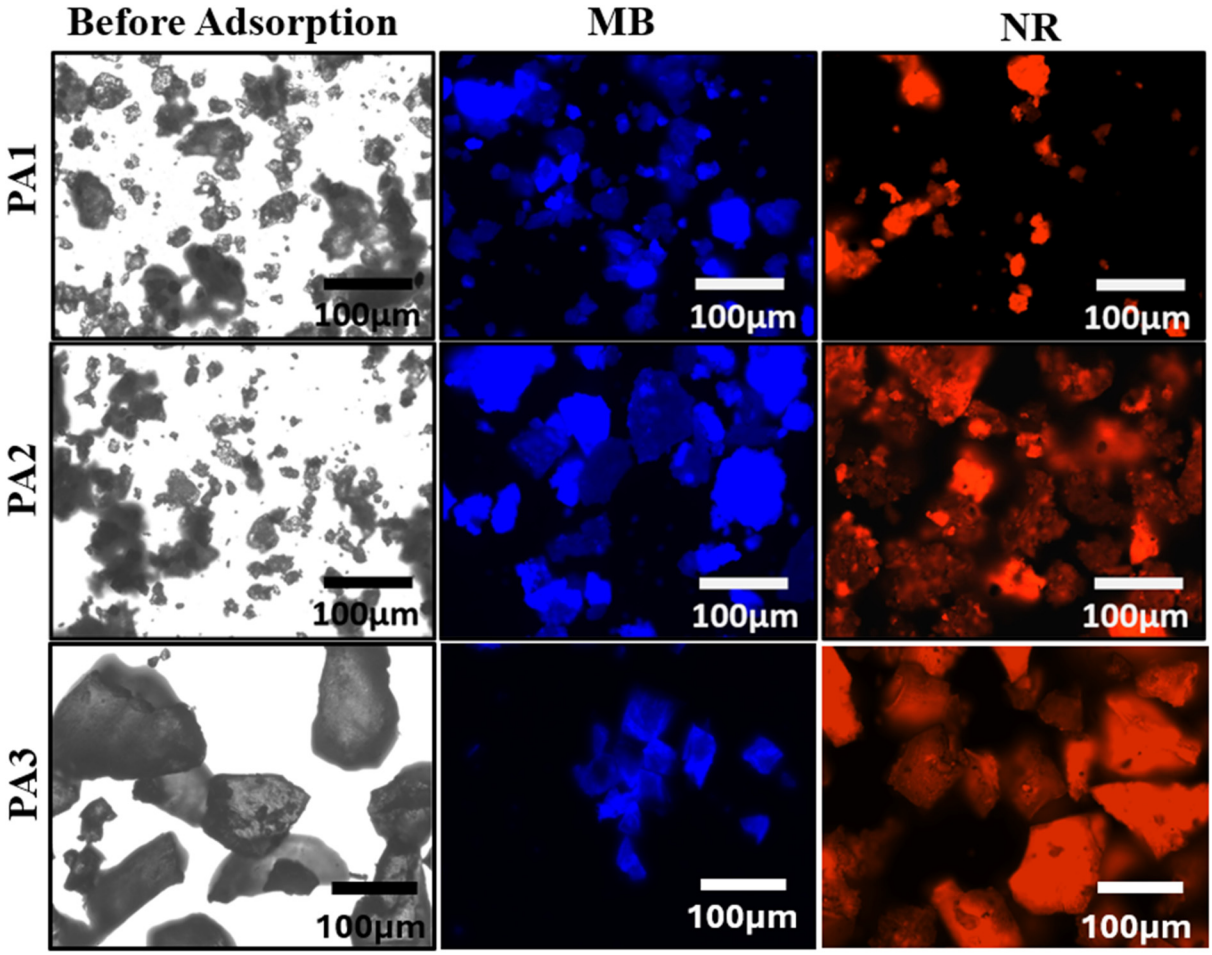

Fig. 6 Optical images of PA1, PA2, and PA3 before and after the adsorption of the dyes MB and NR from solution. The blue emission in the DAPI mode for MB and the red emission in the Texas Red mode for NR were used for optical imaging.

and MB, respectively, compared to the other two PAs (Table 1). The Langmuir model fits the data better than the Freundlich model, as indicated by the data plots (Fig. S10a–f) and the statistical parameters. The values of K_L and n indicate strong adsorption of PVC NPs, NR, and MB on the surface of PAs. The value of the Freundlich constant $n > 1$ indicates that PVC NPs are strongly adsorbed on the surface of the prepared PAs. Due to the strong electrostatic interaction between the PAs and the positively charged pollutants ((+)NPs, NR, and MB), formation of a homogeneous monolayer of the pollutants on the surface of PA was supported by the Langmuir model.

Kinetic studies of adsorption

The data collected using a time-dependent study of the adsorption of (+)PVC NPs and dyes (*i.e.* NR and MB) on the surface of the PAs were analyzed using both pseudo-first-order and pseudo-second-order models. Similar studies were reported for the triazine polymer for the extraction of MB (removal efficiency 90%) with pseudo-second-order kinetics fittings.[51] Fig. 7b, d and f show the highest R^2 values for PAs based on pseudo-second-order kinetics. The pseudo-first-order kinetic regression plots are given in Fig. S10b, d and f.

The theoretical adsorption efficiency ($Q_{e,\ cal}$) calculated from the pseudo-second-order model matched with the experimental value ($Q_{e,\ exp}$) (Table 2) and showed consistency and high value as compared to the values obtained from the data analyzed using the pseudo-first-order model for all PAs. The calculated adsorption capacity ($Q_{e,\ cal}$) values of PA1 and PA2 were in the range of 277–298 mg g^{-1}. PA3 showed higher removal efficiencies of 333.33 mg g^{-1}, 312 mg g^{-1}, and 303 mg g^{-1} for the three pollutants, PVC NPs, NR, and MB, respectively. Kinetic model plots revealed that pseudo-second-order analyses (Fig. 7b, d and f) fit well as compared to the pseudo-first-order analysis (Fig. S10b, d, f and Table 2) of the collected data. The R^2 values obtained from the pseudo-second-order kinetic model analysis are 0.999, 0.999, and 0.981 for PVC NPs, NR, and MB, respectively (Table 2) for PA3, which are close to unity.

Effect of pH on the adsorption of pollutants

Fig. 8 shows the similarities and differences of the calculated removal efficiencies of different pollutants using PAs at three different pH values (3, 7, and 11). At pH 3, the percentage removal of PVC NPs decreased significantly to 41.7 ± 1.5%, 38.1 ± 0.3%, and 46.9 ± 1.4% for PA1, PA2, and PA3, respectively

© 2025 The Author(s). Published by the Royal Society of Chemistry

Open Access Article. Published on 01 August 2025. Downloaded on 2/5/2026 5:41:45 AM.
This article is licensed under a Creative Commons Attribution-NonCommercial 3.0 Unported Licence.

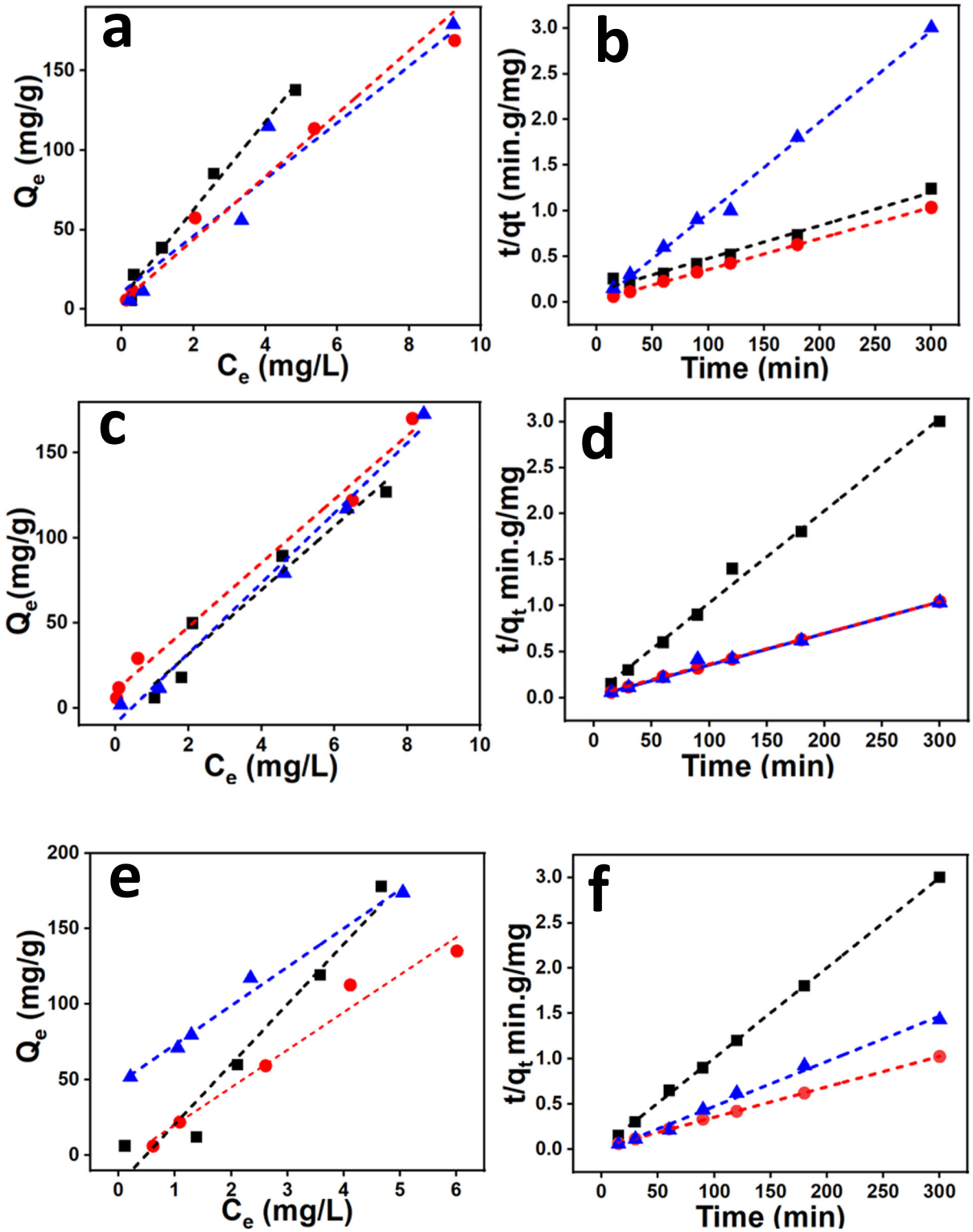

Fig. 7 Langmuir (a, c and e) and pseudo-second-order kinetics (b, d and f) plots of PA1 (a and b), PA2 (c and d), and PA3 (e and f) at room temperature using different concentrations (5–150 mg mL^{-1}) of the (+)PVC NPs (-■-), NR (_●_), and MB (_▲_) and a fixed concentration of PAs (25 mg in 6 mL). The Freundlich isotherms and pseudo-first order kinetic regressions for PA1, PA2, and PA3 are given in the SI (Fig. S10a–f). Regression coefficient and adsorption isotherm parameters for the adsorption of different pollutants ((+)PVC NPs, NR, MB) on the PAs are given in Table 1.

© 2025 The Author(s). Published by the Royal Society of Chemistry

Open Access Article. Published on 01 August 2025. Downloaded on 2/5/2026 5:41:45 AM. This article is licensed under a Creative Commons Attribution-NonCommercial 3.0 Unported Licence.

Table 1 Calculated isotherm parameters for the adsorption of pollutants ((+)PVC NPs, NR, and MB) on the PAs

		Langmuir			Freundlich		
Pollutant	Adsorbent	K_L (L mg^{-1})	Q_{max} (mg g^{-1})	R^2	K_f	n	R^2
(+)PVC NPs	PA1	1.32	29.07	0.987	29.289	1.7889	0.9559
	PA2	2.50	81.30	0.9787	22.067	1.9493	0.9275
	PA3	2.07	83.33	0.9784	22.711	1.381	0.9376
NR	PA1	1.13	85.29	0.9580	14.76	0.9998	0.9395
	PA2	2.37	86.21	0.9777	20.68	1.8135	0.9028
	PA3	0.95	95.06	0.9888	22.501	1.8953	0.9566
MB	PA1	0.14	118.57	0.9840	16.857	1.9409	0.9297
	PA2	0.28	142.85	0.9759	20.017	2.9067	0.9047
	PA3	3.57	157.75	0.9907	21.416	1.9025	0.9025

Table 2 Kinetic parameters for the adsorption of pollutants (PVC NPs, MB, and NR) on the PAs

		Pseudo-first order			Pseudo-second order			
Pollutant	Polyaramide synthesised	Q_e, cal (mg g^{-1})	K_1 (min^{-1})	R^2	Q_e, exp (mg g^{-1})	Q_e, cal (mg g^{-1})	K_2 (min^{-1})	R^2
(+)PVC NPs	PA1	2.72	0.0006	0.9207	286.45	277.78	0.00055	0.9943
	PA2	5.94	0.0005	0.9091	302.12	294.12	0.00042	0.9945
	PA3	5.92	0.0006	0.9095	342.54	333.33	0.00065	0.9997
NR	PA1	42.78	0.0090	0.9530	298.08	294.12	0.00073	0.9980
	PA2	42.49	0.0081	0.9028	299.90	298.51	0.00076	0.9970
	PA3	56.8	0.0150	0.9698	323.57	312.50	0.00015	0.9996
MB	PA1	30.07	0.0065	0.9523	290.99	285.71	0.0017	0.9999
	PA2	27.76	0.0830	0.9047	298.11	287.36	0.0044	0.9759
	PA3	29.27	0.0102	0.9461	312.23	303.03	0.0034	0.9814

(Fig. 8a). At neutral pH 7 and a basic pH 11, the calculated removal efficiencies of the PVC NPs, MB, and NR are in the range of 85–98% for all three polymers (Fig. 8). Protonation of the binding sites of the PAs in the acidic medium reduced the negative charge on the surface and lowered the removal efficiencies of all cationic or neutral pollutants. Guo *et al.* reported that polyaramides prepared from piperazine (PIP) and trimesoyl chloride (TMC) are negatively charged, which is due to the presence of excess acid groups on the surface.[52]

The regeneration of PAs

To understand the recyclability of PAs, regeneration of the adsorbent was done by washing multiple times with dil. HCl solution (10 ml, 0.3 M), followed by water.[11,17] The solid adsorbent was collected and dried before using for the adsorption experiments under similar conditions. The removal efficiency for each extraction was calculated using the absorbance value measured before and after experiments (Fig. 9). The recycled PAs showed almost the same efficiency during the 5 repeating cycles. The pollutants on the surface of PAs are in small quantities and made from ordinary polymers without additives; it is possible to dispose them *via* controlled disposal methods used for plastic waste. Similarly, the regeneration cycles for NR and MB demonstrated that the efficiency was not reduced after 5 cycles, which indicated that the removal efficiencies of PA1, PA2, and PA3 were maintained after 5 cycles.

Successive adsorption study

In most investigations, a single adsorbent was used to extract a specific adsorbate from water. The interactions between the pollutants and the functional groups on the adsorbent surface result in a higher tendency towards adsorption of the pollutants on the PA surface rather than desorption in the equilibrium.[53] Removal of multiple pollutants with a single adsorbent is challenging due to the differences in functional and structural features, as well as affinity for the adsorbent's surface. The synthesized PAs showed interesting surface area, pore size and negative zeta potentials (Table 3), which are useful for the extraction of cationic pollutants from water. To determine the removal efficiency of the PAs towards multiple pollutants, an appropriate amount (25 mg) of PA was used to extract cationic (+)PVC NP solution (6 mL) at an optimum concentration of 50 mg L^{-1}. The removal efficiencies (Fig. 10) and zeta potentials (Table 3) of the PA adsorbents after the extraction were determined. Positive zeta potential values were observed due to the presence of cationic PVC NPs on the surface of PAs, which are denoted as PA1/PVCNP(+), PA2/PVCNP(+), and PA3/PVCNP(+). The observed positive zeta potentials for the PAs were (+)8.34 ± 0.32 mV, (+)8.44 ± 1.73 mV, and (+)12.33 ± 0.33 mV (Table 3). The same adsorbents were used for the next extraction of anionic (−)PVC NPs (6 mL, 50 mg L^{-1}). After 2 h, the mixture was centrifuged, the solids (PA1/PVCNP/PVCNP(−), PA2/PVCNP/PVCNP(−), and

© 2025 The Author(s). Published by the Royal Society of Chemistry

Open Access Article. Published on 01 August 2025. Downloaded on 2/5/2026 5:41:45 AM.
This article is licensed under a Creative Commons Attribution-NonCommercial 3.0 Unported Licence.

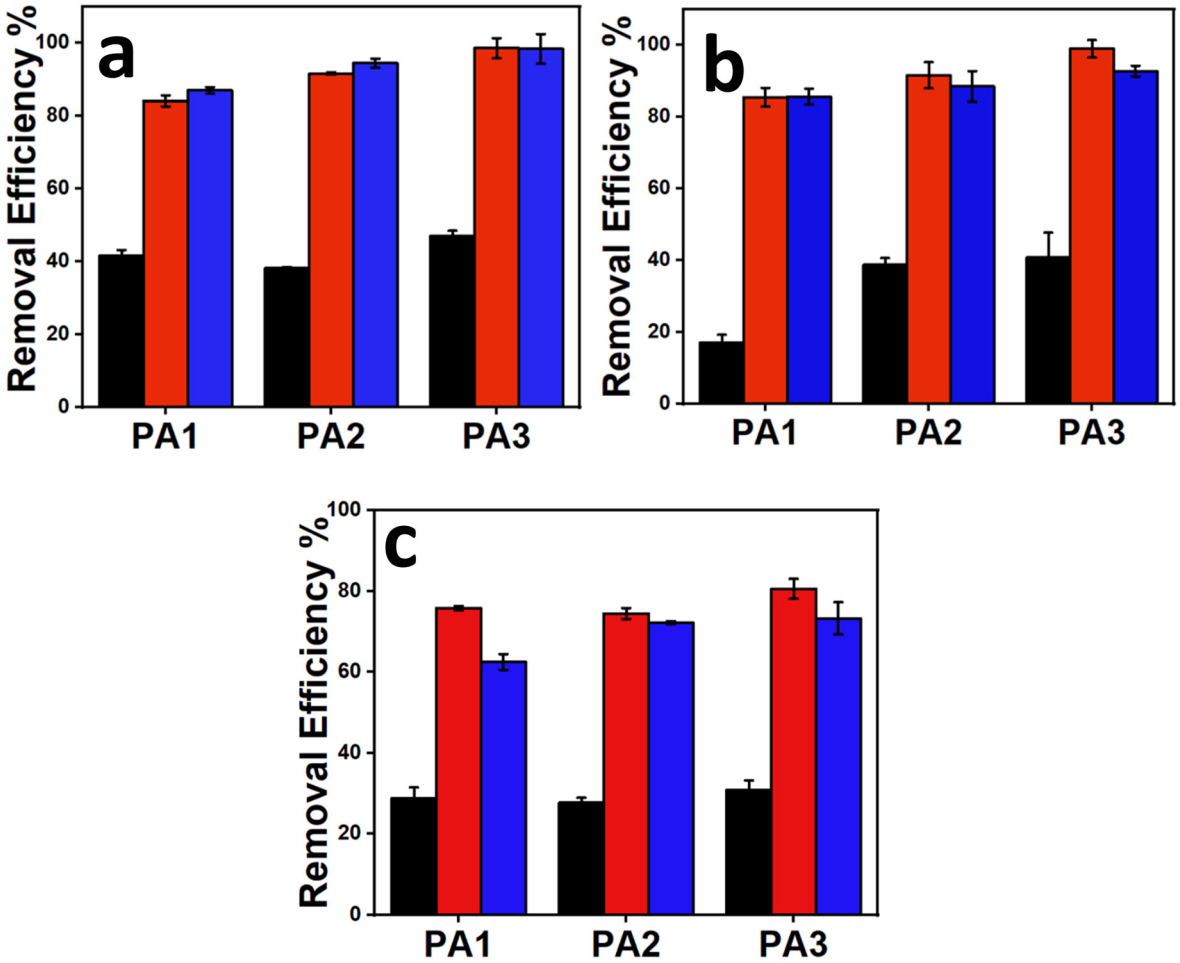

Fig. 8 Removal efficiencies of PAs for the adsorption of (+)PVC NPs (a), NR (b) and MB (c) from water at pH 3 (■), pH 7 (■), and pH 11 (■).

PA3/PVCNP/PVCNP(−)) collected were dispersed in water, and their zeta potential was measured. The zeta potentials observed were (−)12.04 ± 0.04 mV, (−)14.15 ± 0.43 mV, and (−)19.36 ± 0.92 mV (Table 3) with an average removal efficiency in the range of 74.1 ± 2.4–91.6 ± 1.9%. The same solids were used for the third successive extraction of the cationic dye, MB. All PAs showed removal efficiencies in the range of 80.9 ± 1.9–87.5 ± 2.7% for cationic MB. After adsorption, PAs showed the positive zeta potential value of (+)8.75 ± 1.28 mV for PA1/PVCNP/PVCNP/MB(+), (+)8.49 ± 0.36 mV for PA2/PVCNP/PVCNP/MB(+), and (+)11.58 ± 0.30 mV for PA1/PVCNP/PVCNP/MB(+), which implies the adsorption and accumulation of the cationic dye on the surface of the adsorbent. The indicated charges (+ or −) are based on the zeta potential measurements of the adsorbent after each experiment. The optical images of PAs after adsorption of both cationic and anionic pollutants are given in the SI (Fig. S9, S11 and S12).

Similar experiments were also conducted with linear polyaramides (P4, P5, and TA) to assess their successive adsorption efficiencies for pollutants. The results (Fig. 10b) show that PA4 has a greater removal efficiency (88 ± 1.3%) than other linear polymers (PA5 and TA). However, it is significantly lower than the branched polymer, PA3 (99%). Linear polymers, PA5 (66.5 ± 1.6%) and TA (53.1 ± 1.4%), showed low removal efficiencies, which reduced further to 40.5 ± 3.5% and 32 ± 1.98%, respectively, for MB adsorption (Fig. 10b). The changes in the zeta potential also show that linear polymers are able to adsorb cationic and anionic pollutants alternatively based on the net surface charges; however, they were less efficient than the branched polymer.

Adsorption of polymer particles from commercial samples using PAs

Small polymer particles called micro- and nanoplastic particles are accumulating in our water reservoirs due to an increase in plastic waste in the environment.[54] The polymer particles present in a commercial facial scrubber were removed and fully characterized using FTIR spectroscopy. The peaks observed in the spectra were compared with the ingredients listed on the product. The sharp peaks appeared at 2842 cm^{-1} and 2922 cm^{-1}, suggesting that the facial scrubber exhibits a vibrational mode associated with the $>CH_2$ groups present on both surfactants and PP beads (Fig. 11a). Peak positions appeared at 570 cm^{-1}, 718 cm^{-1} (C–C stretching), 1045 cm^{-1}

© 2025 The Author(s). Published by the Royal Society of Chemistry

Open Access Article. Published on 01 August 2025. Downloaded on 2/5/2026 5:41:45 AM.
This article is licensed under a Creative Commons Attribution-NonCommercial 3.0 Unported Licence.

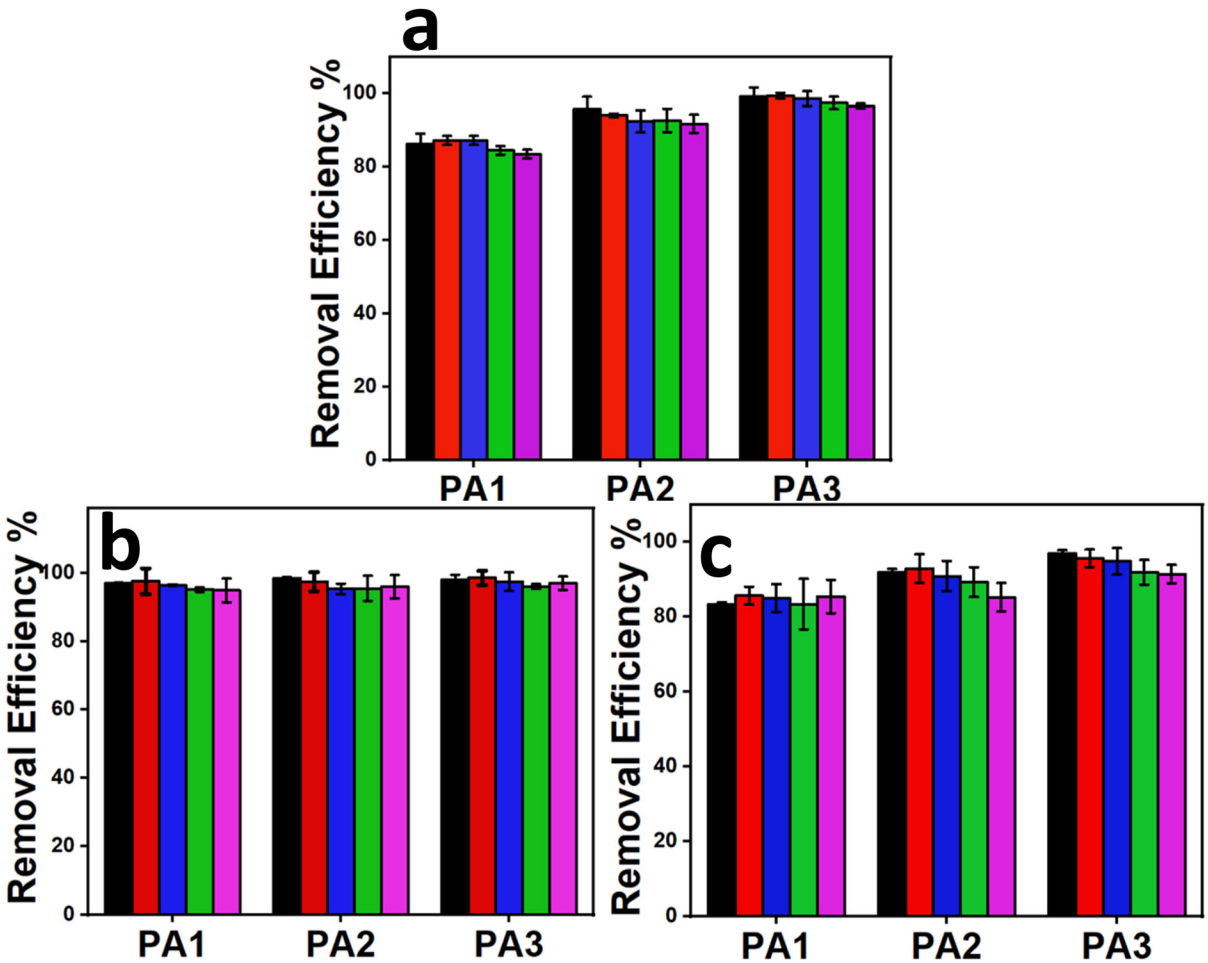

Fig. 9 Removal efficiency of PAs after repeated five adsorption–desorption cycles (cycle 1 (■), cycle 2 (■), cycle 3 (■), cycle 4 (■), and cycle 5 (■)). The concentration of (+) PVC NPs (a), NR (b), MB (c) (50 mg L^{-1}), time (300 min), and adsorbent dose (25 mg) were kept constant.

Table 3 Structural properties and changes in surface potential in the presence of various adsorbed particles or dyes on the surface of PAs

Structural properties of PAs				Zeta potential (mV)			
				Before adsorption	After adsorption		
	Particle size (nm)	Pore size (nm)	Surface area (m^2 g^{-1})		(+)PVC NPs	(−)PVC NPs	MB
PA1	1288 ± 3.09	4.191	10.843	−7.73 ± 1.11	8.34 ± 0.32	−12.04 ± 0.04	8.75 ± 1.28
PA2	918 ± 3.26	2.978	14.048	−13.76 ± 0.38	8.44 ± 1.73	−14.15 ± 0.43	8.49 ± 0.36
PA3	875 ± 1.24	3.233	29.233	−18.87 ± 0.75	12.33 ± 0.33	−19.36 ± 0.92	11.58 ± 0.3
PA4	767 ± 2.16	5.093	6.233	−4.98 ± 0.26	10.48 ± 0.38	−13.54 ± 0.51	7.31 ± 0.08
PA5	864 ± 1.41	3.233	10.315	−7.95 ± 0.33	7.43 ± 0.09	−11.08 ± 0.73	5.38 ± 0.11
TA	529 ± 3.09	5.790	5.683	−2.67 ± 0.53	9.38 ± 0.21	−5.80 ± 0.86	3.08 ± 0.42

Pore size distribution data were extracted from the N_2 adsorption isotherm at 77 K at a pressure of 1 atm (Fig. S13a and b). To measure the particle size, the PAs (0.1 g) were dispersed in water and used for the DLS measurement.

(S═O symmetric stretching), and 1221 cm^{-1} (>S═O antisymmetric stretching), indicating the presence of surfactant molecules[55] (Fig. 11a). A peak appeared at 1398 cm^{-1} due to the C–N stretching mode vibration of the facial scrubber additive such as EDTA.[56] Peak positions between 1638 cm^{-1} and 1720 cm^{-1} appeared due to the >C═O stretching vibrations of the amide and ester groups in the acrylate polymer present in the facial scrubber, respectively. The presence of prominent peaks at 718 cm^{-1} and 1032 cm^{-1} is due to the C–C bond vibrations of the molecules and PP present (Fig. 11a).[57] The

© 2025 The Author(s). Published by the Royal Society of Chemistry

Open Access Article. Published on 01 August 2025. Downloaded on 2/5/2026 5:41:45 AM. This article is licensed under a Creative Commons Attribution-NonCommercial 3.0 Unported Licence.

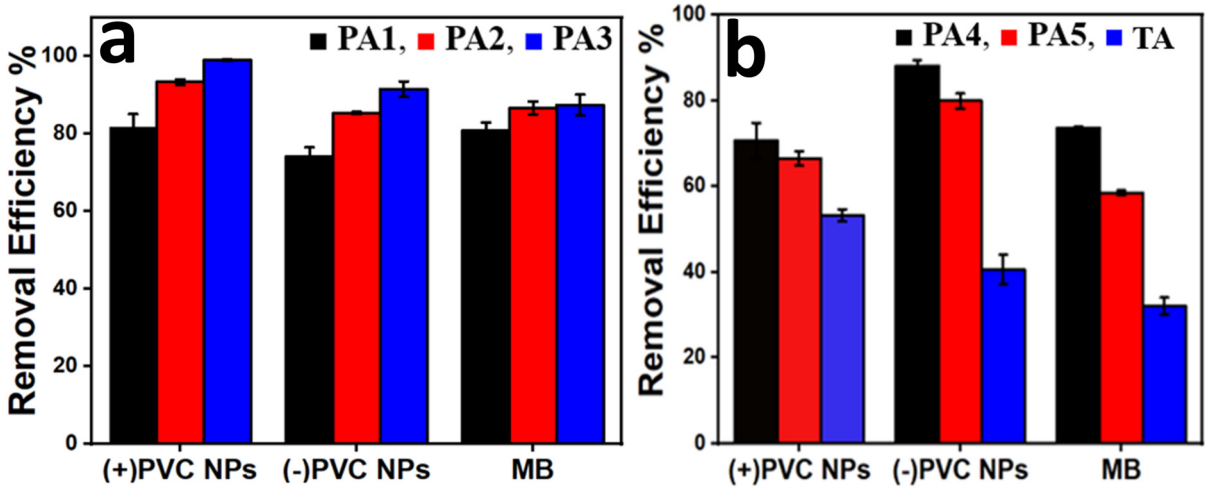

Fig. 10 Successive adsorption studies of oppositely charged pollutants using PAs 1–3 (a), PAs 4,5 and TA (b) and different pollutants (+) PVC NPs and (–)PVC NPs and MB.

peaks observed at 1372 cm^{-1} and 1466 cm^{-1} indicate that the C–H rocking vibrations of the methyl groups of the polypropylene (PP) backbone.[58]

The UV-Vis spectra (Fig. 11b) of the facial scrubber revealed a maximum absorption at 270 nm due to the presence of organic compounds in the scrubber.[59] After the removal of the scrubber, the filtrate was used for absorbance measurement to calculate the removal efficiencies of all PAs. The optical images of the commercial facial scrubber (Fig. 11c,i–iii) showed many PP beads.

To understand the removal efficiency of the microplastic particles from commercial facial scrubber solution, appropriate amounts of PAs (25 mg) and commercial facial scrub solution (50 mg L^{-1}) were used for the extraction experiment. In short, the selected PA (25 mg) was added to the facial scrubber solution (6 ml, 50 mg L^{-1}), and the mixture was shaken for 2 and 5 h to determine the efficiency of PAs. Following a 2 h period of adsorption (Fig. 12a), PAs 1–3 exhibited removal efficiencies of 48.8% ± 3.1, 69.3 ± 4.9%, and 76.7 ± 1.7%, respectively. After 5 h, the removal efficiency of the PAs increased to 73.1 ± 3.1%, 83.8 ± 1.5%, and 97.9 ± 0.4% for PA1, PA2, and PA3, respectively. PA3 showed high removal efficiency as compared to other PAs. The FTIR spectrum of a virgin commercial facial scrubber before adsorption (Fig. 12b, i) was compared to PAs 1–3 after adsorption. Peak positions at 570 cm^{-1} (S–O symmetric stretching), 718 cm^{-1} (C–H bending), 1045 (O–H stretching) cm^{-1}, and 1221 cm^{-1} (C–O stretching) are observed due to the presence of different chemical components present in the facial scrubber (Fig. 12b, ii–iv).[60] The peaks at 2922 cm^{-1}, 2854 cm^{-1} (C–H stretching), and 1372 cm^{-1} (C–H rocking) showed the presence of aliphatic C–H bonds on the PP polymer backbone or aliphatic molecules in the scrubber. According to the above data, it is clear that the components of a commercial facial scrubber are easily removed significantly from the aqueous solution (~98%) by the PA polymers.

Comparison of the removal efficiencies of PAs with other adsorbents

The removal of contaminants from polluted water has been accomplished using hybrid functional materials, organic, inorganic, metal–organic frameworks (MOFs), and covalent organic frameworks.[18] Several studies have reported a range of approaches (coagulation, co-precipitation, adsorption, electrochemical destruction, oxidation, membrane process, *etc.*) using different conditions and materials for removing pollutants from water.[11] Table 4 provides a summary of the various adsorbents reported in the literature for the removal of various NPs and dyes from water. The thiol functionalized adsorbents were used to remove hazardous contaminants from water.[61] The adsorption based process has limited applications in large-scale water filtration due to its moderate adsorption capacity, accessibility, regeneration, and disposal difficulties. As a result, to improve sorption efficiencies, it is necessary to utilize materials that are effective, readily available, and processable, while also possessing high removal efficiency for pollutants. Polyaramides show higher removal efficiency (99%), recyclability, and multi-pollutant removal efficiencies.

Mechanism of adsorption

Crystalline porous molecular frameworks allow covalent integration of organic units into one, two- and three-dimensional (1D, 2D, and 3D) ordered structures with inherent pores.[66] Both EDA and PXA are linear molecules, and with some approximation, the reaction with TMC is expected to give a 2D-architecture. MXA has a kink-like geometry, which then helps PA3 to have a 3D architecture. All PA adsorbents offer a large surface area, high adsorption capacity, and high selectivity, are easy to regenerate and reuse without any degradation. To understand the removal efficiencies of PA1, PA2, and PA3, structurally linear polymers PA4 and PA5 were synthesized using the same experimental conditions. The synthesized PA1

© 2025 The Author(s). Published by the Royal Society of Chemistry

Open Access Article. Published on 01 August 2025. Downloaded on 2/5/2026 5:41:45 AM.
This article is licensed under a Creative Commons Attribution-NonCommercial 3.0 Unported Licence.

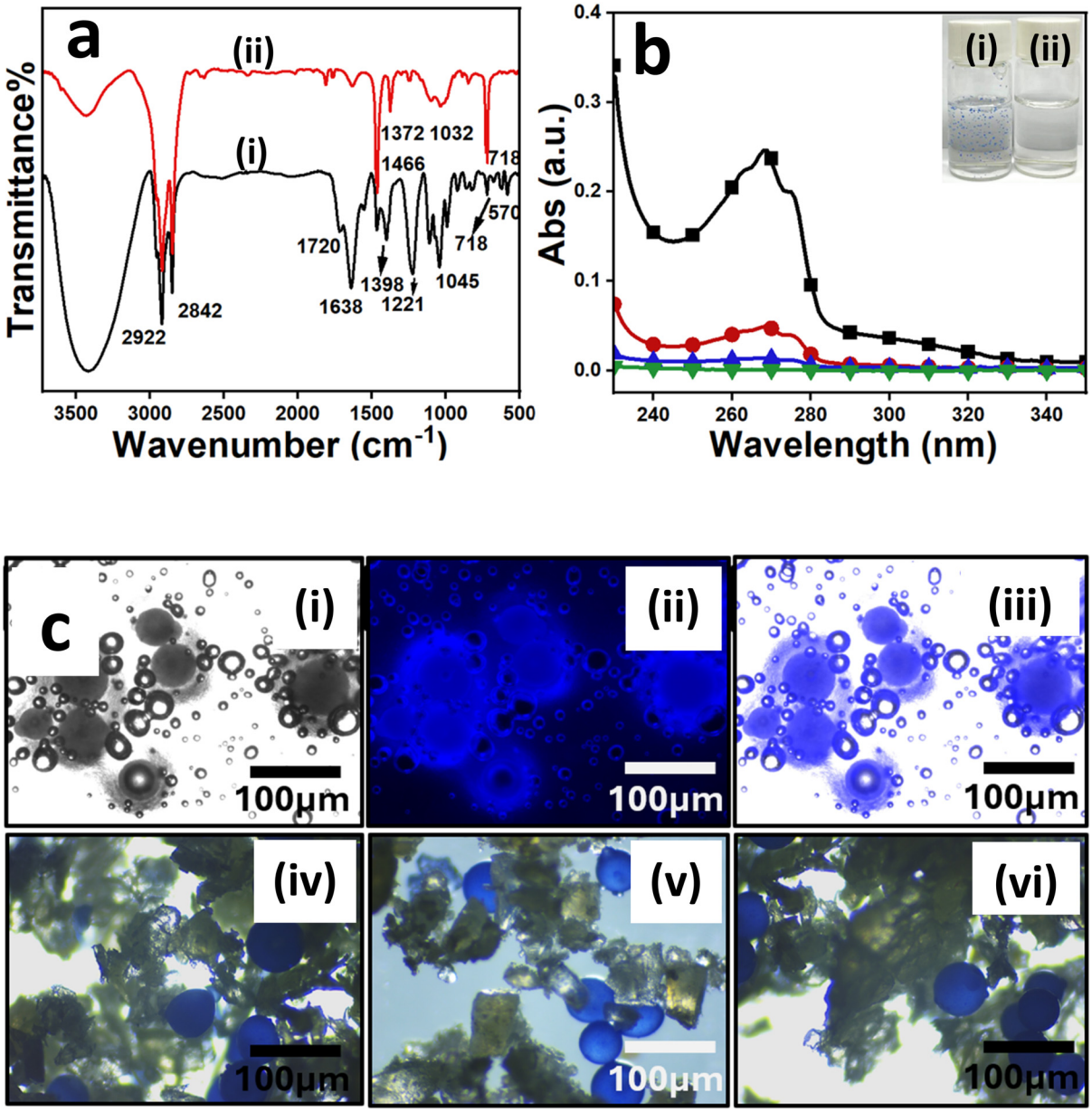

Fig. 11 FTIR spectra (a) of the facial scrubber (i) and blue beads found in the scrubber (ii). UV-Vis spectra (b) of the facial scrubber before (-■-) and after extraction by PA1 (-●-), PA2 (-▲-), PA3 (-▼-). The inset image in (b) indicates the solution of the commercial scrubber before (i) and after (ii) extraction. Optical fluorescence images (c) of polypropylene beads found in a commercial facial scrubber in different modes, such as DIC (i), DAPI (ii), and merged (iii) view of the particles. The air bubbles are seen as circles in the solution. Stereomicroscopic images of the PA1 (iv), PA2 (v), and PA3 (vi) polymers after adsorption of the facial scrubber.

showed a particle size of 1288 ± 3.09 nm, 918 ± 3.26 nm for PA2, and 875 ± 1.24 nm for PA3 (Table 3). Similarly, the particle sizes of linear PA4, PA5, and TA polymers were 767 ± 2.16, 864 ± 1.41, and 529 ± 3.09 nm, respectively. The observed zeta potential of PAs 1–5 dispersed in water was −7.73 ± 1.11 mV, −13.76 ± 0.38 mV, −18.87 ± 0.75 mV, −4.98 ± 0.26 mV, and −7.95 ± 0.33 mV, respectively.

Adsorption techniques have been used to remove contaminants from water. Several variables, such as the concentration and chemical nature of pollutants, pH, contact time, and adsorbent dosage, influence the adsorption behaviour. At a maximum concentration of PAs (25 mg) and an adsorption time of 2 h, high removal rates of 94.05 ± 1.50% (PA1), 89.34 ± 0.50% (PA2), and 99.65 ± 0.03% (PA3) were observed. The linear polyaramides, PA4 and 5, showed removal efficiencies ranging from 72% to 76% for removing nanoparticles and cationic dyes. Similarly, TA was able to remove about 70% of the pollutants that were tested (Fig. S4). The coloured optical images of PAs after adsorption indicate that the +PVC NPs (Fig. S9) were adsorbed on PAs. The zeta potential measure-

© 2025 The Author(s). Published by the Royal Society of Chemistry

Open Access Article. Published on 01 August 2025. Downloaded on 2/5/2026 5:41:45 AM. This article is licensed under a Creative Commons Attribution-NonCommercial 3.0 Unported Licence.

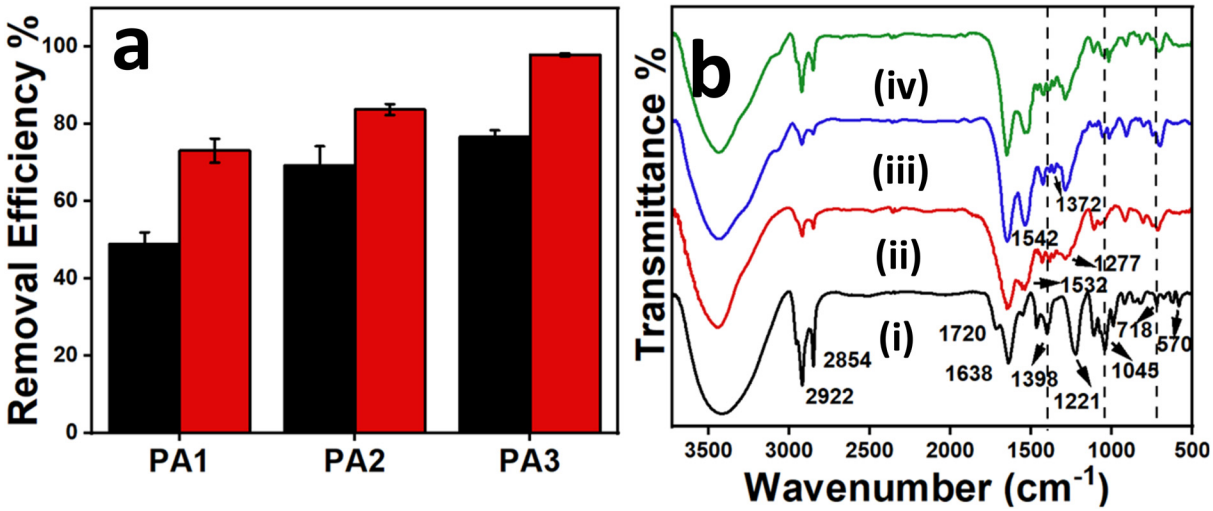

Fig. 12 All PAs (25 mg) were tested for the removal of microplastic particles from the facial scrubber solution. The removal efficiencies (a) of PAs at different time points (■) 2 h and (■) 5 h, and FTIR spectra (b) of the facial scrubber (i) and the scrubber adsorbed on PA1 (ii), PA2 (iii) and PA3 (iv).

Table 4 Comparison of various PAs used for the adsorption of different pollutants from water using different adsorbents

	PA	Adsorbate	Adsorption percentage %	Adsorption efficiency (mg g^{-1})	Ref.
1	TAPB-PDA imine COF	Congo Red	95%	520	62
2	M-COF-SH	Hg(II)	99%	383	61
3	PA-12 nanocomposite	MB and MR	80 and 98%	200.40 and 146.41	45
4	Polyaramide (or nylon)	Paraben	99%	1.44	63
5	p(EDA-TMC)/D composite polymer	RB	—	371.8	64
6	β-Cyclodextrin COF	BPA	98%	—	65
		IBU	99%	—	
7	COF-TP and COF TE	Pb^{2+}	95–96%	149.9	13
8	PA1	PVC NPs, NR and MB	~89%	277–294	This work
9	PA2	PVC NPs, NR and MB	93%	287–298	This work
10	PA3	PVC NPs, NR and MB	99%	312–333	This work
11	PA4	PVC NPs, NR and MB	72%		This work
12	PA5	PVC NPs, NR and MB	75%		This work
13	TA	PVC NPs, NR and MB	70%		This work

ment after adsorption showed positive zeta potential values for all PAs, *i.e.* PA1 (+8.34 ± 0.32), PA2 (+8.44 ± 1.73), PA3 (+12.33 ± 0.33), PA4 (+10.48 ± 0.38) and PA5 (+7.43 ± 0.09) (Table 3) after the adsorption of (+)PVC NPs, which indicates that the adsorption process is electrostatic in nature. The flexibilities and structural geometries of the diamines determine the morphology of the PA backbone. In addition, intra- and intermolecular H-bonds from the PA backbone facilitate the formation of an extensive three-dimensional porous network.[46] The PA3 polymer has trifunctional TMC units linked through a bent difunctional MXA, making the molecule more rigid and 3D; hence, it becomes a 3D molecular structure. For comparing the surface area and pore size of the linear and branched polymers, the adsorption of both nitrogen (N_2) and carbon dioxide (CO_2) gases was used in the BET measurements. The data are shown in Fig. S13 and Table S1. From the N_2 adsorption experiments, the PA1 showed a surface area of 10.483 m^2 g^{-1} and a pore size of 4.191 nm. On the other hand, PA3 showed a high surface area of 29.233 m^2 g^{-1} and a pore diameter of 3.233 nm (Table S1). The pattern of the N_2 adsorption data from BET measurements implies a regular Langmuir monolayer adsorption (Type II) of nitrogen molecules (Fig. S13a and b). Similarly, the CO_2 adsorption experiment gave a surface area of 12.674 m^2 g^{-1} and a pore size of 3.856 nm for PA1 and a large surface area of 35.568 m^2 g^{-1} and a pore diameter of 3.121 nm for PA3 (Table S1). The CO_2 adsorption data imply a type IV multilayer adsorption pattern due to the strong interaction between CO_2 molecules and the polyaramide surface (Fig. S13c and d). We hypothesized that the dye molecules and particles get trapped inside the PA3 lattice as compared to the 2D layered lattices of linear polyaramides.

All PAs followed the Langmuir isotherm and pseudo-second-order-kinetics, with a higher R^2 value (~0.99). An amide-modified clay showed a removal efficiency of 80% for Rhodamine dye with a Q_{max} value of ~371 mg g^{-1}.[64] The

© 2025 The Author(s). Published by the Royal Society of Chemistry

Open Access Article. Published on 01 August 2025. Downloaded on 2/5/2026 5:41:45 AM.
This article is licensed under a Creative Commons Attribution-NonCommercial 3.0 Unported Licence.

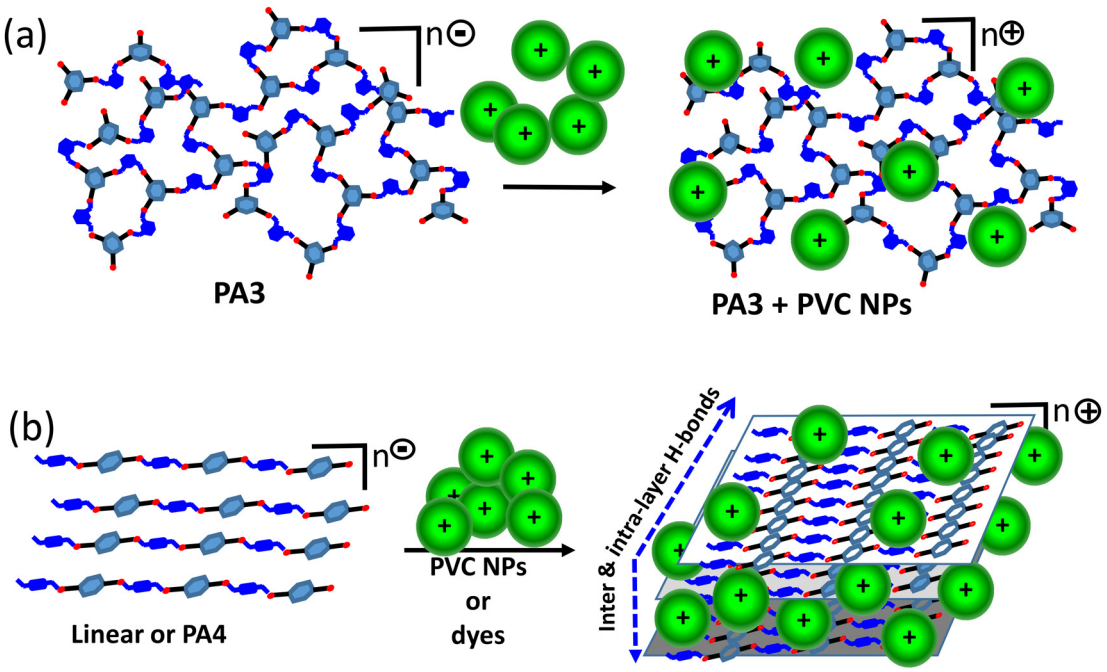

Scheme 2 Schematic representation of the adsorption and removal of PVC NPs by branched networks PA 3 (a) as compared to the linear PA4 or PA5 (b).

observed removal efficiencies of (+)PVC NPs, NR, and MB indicate that strong electrostatic interactions between the negatively charged PA surface and positively charged pollutants are important (Table 3). PA4 and PA5 showed low removal efficiencies, as compared to PA1–3. Similarly, TA showed 30% less efficiency for the removal of pollutants.

The adsorption of organic pollutants on the surface of organic polymers is influenced and facilitated by multiple weak forces such as hydrophobic, electrostatic, and hydrogen bonding interactions.[67,68] To confirm the strong affinity between the adsorbent and adsorbate, negatively charged (–) PVC NPs and anionic methylene orange were also used for the extraction studies and the results indicate that the negatively charged pollutants were not removed from water efficiently (Fig. S14). The higher adsorption efficiencies observed for network PAs are primarily due to the availability of high surface charges, a large number of functional groups, and the presence of hydrated cavities inside the polymer lattice (Scheme 2a), which are not present in linear polymers PA4 and PA5 (Scheme 2b). The porous network structure of PAs facilitates the extraction and retention of the pollutants inside the polymer lattice.

Conclusion

Polyaramides (PAs 1–5, TA) were successfully synthesized using a simple condensation reaction and used for the removal of PVC NPs and different dyes from water. DLS data indicate that all prepared PAs were negatively charged with particle sizes of around 870–1300 nm. Both (+)PVC and (–)PVC NPs with particle sizes of around 120 nm and 135 nm, respectively, were prepared using a nanoprecipitation method and fully characterized. The extractions were done with different concentrations of PVC NPs and dyes, and all PAs had high selectivity towards cationic polymer particles and dyes. Anionic pollutants (*i.e.* (–) PVC NPs and MO) were not adsorbed on the surface and not removed from aqueous solutions. Among the branched PAs 1–3, PA3 showed a high removal efficiency of 99%, while the linear PAs 4 or 5 and TA showed low removal efficiencies of 70–76% for all cationic pollutants investigated. The collected data were fitted with different isotherms and kinetic models to understand the adsorption mechanism. The data fit well with the Langmuir adsorption isotherm and pseudo-second-order kinetics. PA3 showed high Q_{max} values of 83.33, 95.06, and 157.75 mg g^{-1} for PVC NPs, NR, and MB, respectively, compared to the other two PAs. All PAs showed low removal efficiencies at acidic pH 2 and high efficiencies at pH values of 7 and 11. The regeneration and recycling of the PAs were achieved *via* washing with dilute HCl solution and showed no significant decrease in adsorption efficiency after 5 cycles. The PA-based adsorbents reported in this paper are promising, easily accessible candidates for developing large-scale water purification models for emerging pollutants.

Conflicts of interest

There are no conflicts to declare.

© 2025 The Author(s). Published by the Royal Society of Chemistry

Open Access Article. Published on 01 August 2025. Downloaded on 2/5/2026 5:41:45 AM. This article is licensed under a Creative Commons Attribution-NonCommercial 3.0 Unported Licence.

Data availability

The authors confirm that the data supporting this study are available within the article and/or its SI: FTIR spectra, XRD patterns, SEM images and TGA of PA4, PA5, and TA before adsorption; the SEM image of spherical (−)PVC NPs; the effect of adsorbent concentration on removal, UV spectra of (−)PVC NPs, the effect of time and concentrations of pollutants, FTIR spectra of pollutants and adsorbents with pollutants; TGA of the adsorbents after adsorption of pollutants, Freundlich isotherms, optical images of adsorbents after adsorption of individual pollutants, BET data from N_2 and CO_2 adsorption on PA1 and PA3, removal efficiencies of PAs at different concentrations, and comparison of structural properties obtained from N_2 and CO_2 adsorption. See DOI: https://doi.org/10.1039/d5lp00114e.

Acknowledgements

The authors acknowledge the funding support from the National Research Foundation grant A-0004151-00-00 and technical support from the Department of Chemistry at the National University of Singapore.

References

1 C. Fuschi, H. Pu, M. Macdonell, K. Picel, M. Negri and J. Chen, Microplastics in the Great Lakes: Environmental, Health, and Socioeconomic Implications and Future Directions, *ACS Sustainable Chem. Eng.*, 2022, **10**(43), 14074–14091, DOI: 10.1021/acssuschemeng.2c02896.

2 J. Delgado-Gallardo, G. L. Sullivan, P. Esteban, Z. Wang, O. Arar, Z. Li, T. M. Watson and S. Sarp, From Sampling to Analysis: A Critical Review of Techniques Used in the Detection of Micro- and Nanoplastics in Aquatic Environments, *ACS ES&T Water*, 2021, **1**(4), 748–764, DOI: 10.1021/acsestwater.0c00228.

3 M. Hoseini and T. Bond, Predicting the Global Environmental Distribution of Plastic Polymers, *Environ. Pollut.*, 2022, **300**(10), 118966–118976, DOI: 10.1016/j.envpol.2022.118966.

4 A. Schade, M. Melzer, S. Zimmermann, T. Schwarz, K. Stoewe and H. Kuhn, Plastic Waste Recycling—A Chemical Recycling Perspective, *ACS Sustainable Chem. Eng.*, 2024, **12**(33), 12270–12288, DOI: 10.1021/acssuschemeng.4c02551.

5 A. Chamas, H. Moon, J. Zheng, Y. Qiu, T. Tabassum, J. H. Jang, M. Abu-Omar, S. L. Scott and S. Suh, Degradation Rates of Plastics in the Environment, *ACS Sustainable Chem. Eng.*, 2020, **8**(9), 3494–3511, DOI: 10.1021/acssuschemeng.9b06635.

6 X. Zhao and F. You, Microplastic Human Dietary Uptake from 1990 to 2018 Grew across 109 Major Developing and Industrialized Countries but Can Be Halved by Plastic Debris Removal, *Environ. Sci. Technol.*, 2024, **58**(20), 8709–8723, DOI: 10.1021/acs.est.4c00010.

7 Q. Liu, Z. Chen, Y. Chen, F. Yang, W. Yao and Y. Xie, Microplastics and Nanoplastics: Emerging Contaminants in Food, *J. Agric. Food Chem.*, 2021, **69**(36), 10450–10468, DOI: 10.1021/acs.jafc.1c04199.

8 R. Trevisan, C. Voy, S. Chen and R. T. Di Giulio, Nanoplastics, Decrease the Toxicity of a Complex PAH Mixture but Impair Mitochondrial Energy Production in Developing Zebrafish, *Environ. Sci. Technol.*, 2019, **53**(14), 8405–8415, DOI: 10.1021/acs.est.9b02003.

9 G. Mahadevan and S. Valiyaveettil, Comparison of Genotoxicity and Cytotoxicity of Polyvinyl Chloride and Poly(Methyl Methacrylate) Nanoparticles on Normal Human Lung Cell Lines, *Chem. Res. Toxicol.*, 2021, **34**(6), 1468–1480, DOI: 10.1021/acs.chemrestox.0c00391.

10 S. Karan, Z. Jiang and A. G. Livingston, Sub-10 Nm Polyamide Nanofilms with Ultrafast Solvent Transport for Molecular Separation, *Science*, 2015, **348**(6241), 1347–1351, DOI: 10.1126/science.aaa5058.

11 A. Batool and S. Valiyaveettil, Coprecipitation - An Efficient Method for Removal of Polymer Nanoparticles from Water, *ACS Sustainable Chem. Eng.*, 2020, **8**(35), 13481–13487, DOI: 10.1021/acssuschemeng.0c04511.

12 A. Batool and S. Valiyaveettil, Surface Functionalized Cellulose Fibers – A Renewable Adsorbent for Removal of Plastic Nanoparticles from Water, *J. Hazard. Mater.*, 2021, **413**(3), 125301–125311, DOI: 10.1016/j.jhazmat.2021.125301.

13 G. Li, J. Ye, Q. Fang and F. Liu, Amide-Based Covalent Organic Frameworks Materials for Efficient and Recyclable Removal of Heavy Metal Lead(II), *Chem. Eng. J.*, 2019, **370**(1219), 822–830, DOI: 10.1016/j.cej.2019.03.260.

14 N. Huang, L. Zhai, H. Xu and D. Jiang, Stable Covalent Organic Frameworks for Exceptional Mercury Removal from Aqueous Solutions, *J. Am. Chem. Soc.*, 2017, **139**(6), 2428–2434, DOI: 10.1021/jacs.6b12328.

15 D. T. Sun, L. Peng, W. S. Reeder, S. M. Moosavi, D. Tiana, D. K. Britt, E. Oveisi and W. L. Queen, Rapid, Selective Heavy Metal Removal from Water by a Metal-Organic Framework/Polydopamine Composite, *ACS Cent. Sci.*, 2018, **4**(3), 349–356, DOI: 10.1021/acscentsci.7b00605.

16 E. H. Gora, S. G. Saldana, L. M. Casper, V. Coll Sijercic, O. A. Giza and R. L. Sanders, Effect of Exhausted Coffee Ground Particle Size on Metal Ion Adsorption Rates and Capacities, *ACS Omega*, 2022, **7**(43), 38600–38612, DOI: 10.1021/acsomega.2c04058.

17 A. Batool and S. Valiyaveettil, Chemical Transformation of Soya Waste into Stable Adsorbent for Enhanced Removal of Methylene Blue and Neutral Red from Water, *J. Environ. Chem. Eng.*, 2021, **9**(1), 104902–104912, DOI: 10.1016/j.jece.2020.104902.

18 S. Modak, M. Kasula and M. R. Esfahani, Nanoplastics Removal from Water Using Metal–Organic Framework: Investigation of Adsorption Mechanisms, Kinetics, and Effective Environmental Parameters, *ACS Appl. Eng. Mater.*, 2023, **1**(2), 744–755, DOI: 10.1021/acsaenm.2c00174.

© 2025 The Author(s). Published by the Royal Society of Chemistry

Open Access Article. Published on 01 August 2025. Downloaded on 2/5/2026 5:41:45 AM. This article is licensed under a Creative Commons Attribution-NonCommercial 3.0 Unported Licence.

19 N. Dai, X. Liu, L. Yang, X. Huang, D. Song, S. Wang, K. Zhang, X. Liu, W. Dong and Y. Zhang, Cetyltrimethylammonium Bromide-Modified Laponite@Diatomite Composites for Enhanced Adsorption Performance of Organic Pollutants, *Langmuir*, 2024, **40**(16), 8427–8439, DOI: 10.1021/acs.langmuir.3c03938.

20 T. F. Machado, A. J. M. Valente, M. E. S. Serra and D. Murtinho, Triazene-Linked Porous Organic Polymers for Heterogeneous Catalysis and Pollutant Adsorption, *ACS Appl. Polym. Mater.*, 2024, **6**(7), 4171–4185, DOI: 10.1021/acsapm.4c00225.

21 A. Eluri, K. Sairam, J. D. Halpara and N. A. Babujohn, Tuning the Surface Area and Pore Size of Pyrene-Biphenyl-Coupled Hypercross-Linked Polymers to Capture Toxic Organic Pollutants, *ACS Appl. Polym. Mater.*, 2022, **4**(10), 6936–6948, DOI: 10.1021/acsapm.2c00856.

22 K. Liu, M. Fu, X. Ma, P. Zhang, S. Zong and W. Zhao, One-Pot Synthesis of Carboxyl-Functionalized Hyper-Cross-Linked Microporous Polymer Based on the Dual-Purpose Reagent Strategy for the Efficient Removal of Methylene Blue from Water, *ACS Appl. Polym. Mater.*, 2023, **5**(12), 9807–9816, DOI: 10.1021/acsapm.3c01529.

23 H. Liu, F. Tian, B. Gao, W. Wang, Y. Bai, C. Zhang and L. Dong, 3D Covalent Organic Framework Membranes for Molecular Separations, *Chem. – Eur. J.*, 2024, **30**(67), e202402876, DOI: 10.1002/chem.202402876.

24 C. Fan, H. Geng, H. Wu, Q. Peng, X. Wang, B. Shi, Y. Kong, Z. Yin, Y. Liu and Z. Jiang, Three-Dimensional Covalent Organic Framework Membrane for Efficient Proton Conduction, *J. Mater. Chem. A*, 2021, **9**(33), 17720–17723, DOI: 10.1039/d1ta05005b.

25 Y. Yang, Y. Chen, F. Izquierdo-ruiz, S. Clara, M. Rahm and K. Borjesson, A Self-Standing Three-Dimensional Covalent Organic Framework Fi Lm, *Nat. Commun.*, 2023, **14**, 220–229, DOI: 10.1038/s41467-023-35931-4.

26 X. Kong, Z. Wu and C. Xu, Ambient Aqueous Synthesis of Imine-Linked Covalent Organic Frameworks (COFs) and Fabrication of Freestanding Cellulose Nanofiber@COF Nanopapers, *J. Am. Chem. Soc.*, 2024, **146**, 742–751, DOI: 10.1021/jacs.3c10691.

27 T. Shirokura, T. Hirohata, K. Sato, E. Villani, K. Sekiya, Y. A. Chien, T. Kurioka, R. Hifumi, Y. Hattori, M. Sone, I. Tomita and S. Inagi, Site-Selective Synthesis and Concurrent Immobilization of Imine-Based Covalent Organic Frameworks on Electrodes Using an Electrogenerated Acid, *Angew. Chem., Int. Ed.*, 2023, **62**(40), 1–9, DOI: 10.1002/anie.202307343.

28 R. S. Alruwais and W. A. Adeosun, Recent Advances of Copolymer for Water Treatment, *Water Environ. Res.*, 2024, **96**(4), 1–19, DOI: 10.1002/wer.11030.

29 R. Li, J. Zhai, J. Jiang, Q. Wang and S. Wang, Improved Interfacial Ion Transport through Nanofluidic Hybrid Membranes Based on Covalent Organic Frameworks for Osmotic Energy Generation, *ACS Appl. Energy Mater.*, 2022, **5**(6), 7176–7184, DOI: 10.1021/acsaem.2c00734.

30 C. Xiong, H. Wang, L. Deng, K. Liang, C. Wu, W. Wu and Q. Chen, Novel Triazine-Based Sulfur-Containing Polyamides: Preparation, Adsorption Efficiency and Mechanism for Mercury Ions, *Eur. Polym. J.*, 2024, **202**, 112588–112599, DOI: 10.1016/j.eurpolymj.2023.112588.

31 R. S. Khandge, T. T. Nguyen, Z. Qiang, H. K. Yu and X. Ma, Polyamide-Crystalline Covalent Organic Framework Dual-Layer Nanofiltration Membrane with Improved Ion Selectivity, *ACS Appl. Polym. Mater.*, 2024, **6**(22), 13877–13885, DOI: 10.1021/acsapm.4c02850.

32 G. Han, R. M. Studer, M. Lee, K. M. Rodriguez, J. J. Teesdale and Z. P. Smith, Engineering Interfacial Structure and Channels of Polyamide Thin-Film Nanocomposite Membranes to Enhance Permselectivity for Water Purification, *Chem. Mater.*, 2024, **36**(14), 7005–7015, DOI: 10.1021/acs.chemmater.4c01246.

33 C. Li, P. Guggenberger, S. W. Han, W. L. Ding and F. Kleitz, Ultrathin Covalent Organic Framework Anchored on Graphene for Enhanced Organic Pollutant Removal, *Angew. Chem., Int. Ed.*, 2022, **61**(35), 1–7, DOI: 10.1002/anie.202206564.

34 Y. Liang, Y. Zhu, C. Liu, K. Lee, W. Hung, Z. Wang, Y. Li, M. Elimelech, J. Jin and S. Lin, Polyamide Nanofiltration Membrane with Highly Uniform Sub-Nanometre Pores for Sub-1 Å Precision Separation, *Nat. Commun.*, 2020, **11**(2020), 1–9, DOI: 10.1038/s41467-020-15771-2.

35 S. Bhargava, J. J. H. Chu and S. Valiyaveettil, Controlled Dye Aggregation in Sodium Dodecylsulfate-Stabilized Poly (Methylmethacrylate) Nanoparticles as Fluorescent Imaging Probes, *ACS Omega*, 2018, **3**(7), 7663–7672, DOI: 10.1021/acsomega.8b00785.

36 Z. B. Zhou, X. H. Han, Q. Y. Qi, S. X. Gan, D. L. Ma and X. Zhao, A Facile, Efficient, and General Synthetic Method to Amide-Linked Covalent Organic Frameworks, *J. Am. Chem. Soc.*, 2022, **144**(3), 1138–1143, DOI: 10.1021/jacs.1c12392.

37 Y. Lu, Z. B. Zhou, Q. Y. Qi, J. Yao and X. Zhao, Polyamide Covalent Organic Framework Membranes for Molecular Sieving, *ACS Appl. Mater. Interfaces*, 2022, **14**(32), 37019–37027, DOI: 10.1021/acsami.2c07753.

38 A. Waheed, U. Baig and I. H. Aljundi, Fabrication of Polyamide Thin Film Composite Membranes Using Aliphatic Tetra-Amines and Terephthaloyl Chloride Crosslinker for Organic Solvent Nanofiltration, *Sci. Rep.*, 2023, **13**(1), 1–15, DOI: 10.1038/s41598-023-38269-5.

39 S. Cantekin, T. F. A. de Greef and A. R. A. Palmans, Benzene-1,3,5-Tricarboxamide: A Versatile Ordering Moiety for Supramolecular Chemistry, *Chem. Soc. Rev.*, 2012, **41**(18), 6125–6137, DOI: 10.1039/c2cs35156k.

40 G. Mahadevan and S. Valiyaveettil, Understanding the Interactions of Poly(Methyl Methacrylate) and Poly(Vinyl Chloride) Nanoparticles with BHK-21 Cell Line, *Sci. Rep.*, 2021, **11**(1), 1–15, DOI: 10.1038/s41598-020-80708-0.

41 K. Juraij, S. P. Ammed, C. Chingakham, B. Ramasubramanian, S. Ramakrishna, S. Vasudevan and A. Sujith, Electrospun Polyurethane Nanofiber Membranes for Microplastic and Nanoplastic Separation, *ACS Appl. Nano Mater.*, 2023, **6**(6), 4636–4650, DOI: 10.1021/acsanm.3c00112.

© 2025 The Author(s). Published by the Royal Society of Chemistry

Open Access Article. Published on 01 August 2025. Downloaded on 2/5/2026 5:41:45 AM. This article is licensed under a Creative Commons Attribution-NonCommercial 3.0 Unported Licence.

42 M. Feng, W. You, Z. Wu, Q. Chen and H. Zhan, Mildly Alkaline Preparation and Methylene Blue Adsorption Capacity of Hierarchical Flower-like Sodium Titanate, *ACS Appl. Mater. Interfaces*, 2013, **5**(23), 12654–12662, DOI: 10.1021/am404011k.

43 I. Langmuir, Adsorption of Gases on Glass,Mica and Platinum, *J. Am. Chem. Soc.*, 1919, **40**(1914), 1361–1403, DOI: 10.1021/ja02242a004.

44 D. V. Volodkin, A. I. Petrov, M. Prevot and G. B. Sukhorukov, Matrix Polyelectrolyte Microcapsules: New System for Macromolecule Encapsulation, *Langmuir*, 2004, **20**(8), 3398–3406, DOI: 10.1021/la036177z.

45 S. A. Aldahash, P. Higgins, S. Siddiqui and M. K. Uddin, Fabrication of Polyamide-12/Cement Nanocomposite and Its Testing for Different Dyes Removal from Aqueous Solution: Characterization, Adsorption, and Regeneration Studies, *Sci. Rep.*, 2022, **12**(1), 13144–13163, DOI: 10.1038/s41598-022-16977-8.

46 V. M. Suresh, S. Bonakala, H. S. Atreya, S. Balasubramanian and T. K. Maji, Amide Functionalized Microporous Organic Polymer (Am-MOP) for Selective CO2 Sorption and Catalysis, *ACS Appl. Mater. Interfaces*, 2014, **6**(7), 4630–4637, DOI: 10.1021/am500057z.

47 N. A. Khan, N. A. Khan, N. A. Khan, J. Yuan, J. Yuan, H. Wu, H. Wu, H. Wu, T. Huang, T. Huang, X. You, X. You, A. U. Rahman, C. S. Azad, M. A. Olson, M. A. Olson, Z. Jiang and Z. Jiang, Covalent Organic Framework Nanosheets as Reactive Fillers to Fabricate Free-Standing Polyamide Membranes for Efficient Desalination, *ACS Appl. Mater. Interfaces*, 2020, **12**(24), 27777–27785, DOI: 10.1021/acsami.0c06417.

48 I. S. Ryu, X. Liu, Y. Jin, J. Sun and Y. J. Lee, Stoichiometric Analysis of Competing Intermolecular Hydrogen Bonds Using Infrared Spectroscopy, *RSC Adv.*, 2018, **8**(42), 23481–23488, DOI: 10.1039/c8ra02919a.

49 Y. F. Zhang, P. Z. Zhou, L. H. Guo and H. H. Hou, The Relationship between Crystal Structure and Nucleation Effect of 1,3,5-Benzenetricarboxylic Acid Tris(Phenylamide) in Isotactic Polypropylene, *Colloid Polym. Sci.*, 2017, **295**(4), 619–626, DOI: 10.1007/s00396-017-4030-z.

50 S. Cho, J. H. Kim, K. S. Yang and M. Chang, Facile Preparation of Amino-Functionalized Polymeric Microcapsules as Efficient Adsorbent for Heavy Metal Ions Removal, *Chem. Eng. J.*, 2021, **425**(12), 130645–130653, DOI: 10.1016/j.cej.2021.130645.

51 J. Huo, B. Luo and Y. Chen, Crystalline Covalent Organic Frameworks from Triazine Nodes as Porous Adsorbents for Dye Pollutants, *ACS Omega*, 2019, **4**(27), 22504–22513, DOI: 10.1021/acsomega.9b03176.

52 B. B. Guo, C. Liu, C. Y. Zhu, J. H. Xin, C. Zhang, H. C. Yang and Z. K. Xu, Double Charge Flips of Polyamide Membrane by Ionic Liquid-Decoupled Bulk and Interfacial Diffusion for on-Demand Nanofiltration, *Nat. Commun.*, 2024, **15**(1), 1–11, DOI: 10.1038/s41467-024-46580-6.

53 A. Batool and S. Valiyaveettil, Sequential Removal of Oppositely Charged Multiple Compounds from Water Using Surface-Modified Cellulose, *Ind. Eng. Chem. Res.*, 2022, **61**(1), 716–726, DOI: 10.1021/acs.iecr.1c03847.

54 A. O. C. Iroegbu, S. S. Ray, V. Mbarane, J. C. Bordado and J. P. Sardinha, Plastic Pollution: A Perspective on Matters Arising: Challenges and Opportunities, *ACS Omega*, 2021, **6**(30), 19343–19355, DOI: 10.1021/acsomega.1c02760.

55 A. Hethnawi, T. Karaki, Y. Z. Keteklahijani, M. Chehelamirani, A. Hassan and N. N. Nassar, Enhanced Settling and Dewatering of Oil Sands Mature Fine Tailings with Titanomagnetite Nanoparticles Grafted with Polyacrylamide and Lauryl Sulfate, *ACS Appl. Nano Mater.*, 2022, **5**(6), 7679–7695, DOI: 10.1021/acsanm.1c04566.

56 L. Yang, P. W. May, L. Yin, J. A. Smith and K. N. Rosser, Ultra Fine Carbon Nitride Nanocrystals Synthesized by Laser Ablation in Liquid Solution, *J. Nanopart. Res.*, 2007, **9**(6), 1181–1185, DOI: 10.1007/s11051-006-9192-4.

57 K. I. Hadjiivanov, D. A. Panayotov, M. Y. Mihaylov, E. Z. Ivanova, K. K. Chakarova, S. M. Andonova and N. L. Drenchev, Power of Infrared and Raman Spectroscopies to Characterize Metal-Organic Frameworks and Investigate Their Interaction with Guest Molecules, *Chem. Rev.*, 2021, **121**(3), 1286–1424, DOI: 10.1021/acs.chemrev.0c00487.

58 K. Zheng, R. Liu, H. Chang, D. Shen and Y. Huang, In Situ FTIR Spectroscopic Study of the Conformational Change of Syndiotactic Polypropylene during the Isothermal Crystallization, *Polymer*, 2009, **50**(24), 12461–12463, DOI: 10.1016/j.polymer.2009.10.017.

59 K. Akhter, K. Ullah, R. Talat, A. Haider, N. Khalid, F. Ullah and S. Ali, Synthesis and Characterization of Cationic Surfactants and Their Interactions with Drug and Metal Complexes, *Heliyon*, 2019, **5**(6), 1–8, DOI: 10.1016/j.heliyon.2019.e01885.

60 I. Azamian, S. R. Allahkaram and S. Rezaee, Autonomous-Healing and Smart Anti-Corrosion Mechanism of Polyurethane Embedded with a Novel Synthesized Microcapsule Containing Sodium Dodecyl Sulfate as a Corrosion Inhibitor, *RSC Adv.*, 2022, **12**(22), 14299–14314, DOI: 10.1039/d2ra01131j.

61 L. Huang, R. Shen, R. Liu and Q. Shuai, Thiol-Functionalized Magnetic Covalent Organic Frameworks by a Cutting Strategy for Efficient Removal of Hg2 + from Water, *J. Hazard. Mater.*, 2020, **392**(2), 122320–122328, DOI: 10.1016/j.jhazmat.2020.122320.

62 J. L. Fenton, D. W. Burke, D. Qian, M. O. D. L. Cruz and W. R. Dichtel, Polycrystalline Covalent Organic Framework Films Act as Adsorbents, Not Membranes, *J. Am. Chem. Soc.*, 2021, **143**(3), 1466–1473, DOI: 10.1021/jacs.0c11159.

63 C. Mejías, J. Martín, J. L. Santos, I. Aparicio and E. Alonso, Role of Polyamide Microplastics as Vector of Parabens in the Environment: An Adsorption Study, *Environ. Technol. Innovation*, 2023, **32**(1), 103276–103289, DOI: 10.1016/j.eti.2023.103276.

64 T. A. Saleh, M. Tuzen and A. Sarı, Evaluation of Poly (Ethylene Diamine-Trimesoyl Chloride)-Modified Diatomite as Efficient Adsorbent for Removal of

Open Access Article. Published on 01 August 2025. Downloaded on 2/5/2026 5:41:45 AM.
This article is licensed under a Creative Commons Attribution-NonCommercial 3.0 Unported Licence.

Rhodamine B from Wastewater Samples, *Environ. Sci. Pollut. Res.*, 2021, **28**(39), 55655–55666, DOI: 10.1007/s11356-021-14832-3.

65 M. K. Jørgensen, D. Deemter, L. W. Städe, L. G. Sørensen, L. N. Madsen, I. Oller, S. Malato, T. T. Nielsen and V. Boffa, High Performance Ultra- and Nanofiltration Removal of Micropollutants by Cyclodextrin Complexation, *Chem. Eng. Res. Des.*, 2022, **188**(6), 694–703, DOI: 10.1016/j.cherd.2022.10.026.

66 J. Guo and D. Jiang, Covalent Organic Frameworks for Heterogeneous Catalysis: Principle, Current Status, and Challenges, *ACS Cent. Sci.*, 2020, **6**(6), 869–879, DOI: 10.1021/acscentsci.0c00463.

67 P. Qi, J. Wang, H. Li, Y. Wu, Z. Liu, B. Zheng and X. Wang, Fluffy Ball-like Magnetic Covalent Organic Frameworks for Adsorption and Removal of Organothiophosphate Pesticides, *Sci. Total Environ.*, 2022, **840**(198), 156529–156539, DOI: 10.1016/j.scitotenv.2022.156529.

68 J. B. Feng, Y. y. Li, Y. Zhang, Y. y. Xu and X. W. Cheng, Adsorptive Removal of Indomethacin and Diclofenac from Water by Polypyrrole Doped-GO/COF-300 Nanocomposites, *Chem. Eng. J.*, 2022, **429**(17), 132499–132515, DOI: 10.1016/j.cej.2021.132499.

© 2025 The Author(s). Published by the Royal Society of Chemistry